PLOS BIOLOGY

RESEARCH ARTICLE

microRNA-142 guards against autoimmunity by controlling T_{reg} cell homeostasis and function

Wei-Le Wang[1,2], Ching Ouyang[3,4], Natalie M. Graham[1,2], Yuankun Zhang[5], Kaniel Cassady[1,5], Estefany Y. Reyes[2], Min Xiong[1,2], Alicia M. Davis[1], Kathie Tang[2], Defu Zeng[1,5], Mark P. Boldin[1,2]*

1 Irell and Manella Graduate School of Biological Sciences, Beckman Research Institute, City of Hope, Duarte, California, United States of America, **2** Department of Systems Biology, Beckman Research Institute, City of Hope, Duarte, California, United States of America, **3** Center for Informatics, Beckman Research Institute, City of Hope, Duarte, California, United States of America, **4** Department of Computational and Quantitative Medicine, Beckman Research Institute, City of Hope, Duarte, California, United States of America, **5** Department of Diabetes Research, Beckman Research Institute, City of Hope, Duarte, California, United States of America

* mboldin@coh.org

Citation: Wang W-L, Ouyang C, Graham NM, Zhang Y, Cassady K, Reyes EY, et al. (2022) *microRNA-142* guards against autoimmunity by controlling T_{reg} cell homeostasis and function. PLoS Biol 20(2): e3001552. https://doi.org/10.1371/journal.pbio.3001552

Academic Editor: Paula M. Oliver, Children's Hospital of Philadelphia and The University of Pennsylvania School of Medicine, UNITED STATES

Received: November 10, 2021

Accepted: January 21, 2022

Published: February 18, 2022

Data Availability Statement: The underlying raw data can be found within the paper and its Supporting Information files. The RNA-seq data used in the paper are publicly available from the GEO database (accession number GSE190192). The underlying flow cytometry raw data can be found at the Figshare data repository (https://figshare.com/projects/microRNA-142_guards_against_autoimmunity_by_controlling_Treg_cell_homeostasis_and_function/128960).

Abstract

Regulatory T (T_{reg}) cells are critical in preventing aberrant immune responses. Posttranscriptional control of gene expression by microRNA (miRNA) has recently emerged as an essential genetic element for T_{reg} cell function. Here, we report that mice with T_{reg} cell–specific ablation of *miR-142* (hereafter *Foxp3*^{Cre}*miR-142*$^{fl/fl}$ mice) developed a fatal systemic autoimmune disorder due to a breakdown in peripheral T-cell tolerance. *Foxp3*^{Cre}*miR-142*$^{fl/fl}$ mice displayed a significant decrease in the abundance and suppressive capacity of T_{reg} cells. Expression profiling of *miR-142*–deficient T_{reg} cells revealed an up-regulation of multiple genes in the interferon gamma (IFNγ) signaling network. We identified several of these IFNγ-associated genes as direct miR-142-3p targets and observed excessive IFNγ production and signaling in *miR-142*–deficient T_{reg} cells. *Ifng* ablation rescued the T_{reg} cell homeostatic defect and alleviated development of autoimmunity in *Foxp3*^{Cre}*miR-142*$^{fl/fl}$ mice. Thus, our findings implicate *miR-142* as an indispensable regulator of T_{reg} cell homeostasis that exerts its function by attenuating IFNγ responses.

Introduction

Regulatory T (T_{reg}) cells are vital in maintaining immune self-tolerance and restraining aberrant immune responses against infections [1,2]. *Foxp3*, an X chromosome–linked member of the forkhead box/winged helix family of transcription factors, is a master regulator of the genetic program that governs development and suppressive activity of T_{reg} cells. Humans and mice that carry loss-of-function *Foxp3* mutations develop a fatal autoimmune disease due to impaired T_{reg} cell activity [3–7]. The majority of T_{reg} cells are generated in the thymus (tT_{reg} cells) through a selection process that favors cells with a strong functional T cell receptor

Funding: This study was funded in part by the National Institute of Allergy and Infectious Diseases of the National Institutes of Health R01 AI125615 (to M. P. B.) and R01 AI146313 (to M. P. B.) grants and the American Association of Immunologists Careers in Immunology Fellowship (to M. P. B. and W. L. W.). The work in the Zeng lab was supported by the National Cancer Institute of the National Institutes of Health R01 CA228465 grant (to D. Z.). Research reported in this publication includes work performed in the Analytical Cytometry, Integrative Genomics and Veterinary Pathology Cores supported by the National Cancer Institute of the National Institutes of Health under P30 CA033572 award (to City of Hope Comprehensive Cancer Center). The funders had no role in study design, data collection and analysis, decision to publish, or preparation of the manuscript.

Competing interests: The authors have declared that no competing interests exist.

Abbreviations: Ab, antibody; aGVHD, acute graft-versus-host disease; BMT, bone marrow transplantation; BrdU, 5-bromo-2-deoxyuridine; CPM, counts per million; CTLA4, cytotoxic T-lymphocyte associated protein 4; CTV, CellTrace Violet; DC, dendritic cell; DP, double positive; FACS, fluorescence activated cell sorting; FDR, false discovery rate; GITR, glucocorticoid-induced tumor necrosis factor receptor family-related gene; GLM, generalized linear model; GSEA, Gene Set Enrichment Analysis; Hif1a, hypoxia-induced factor 1 alpha; HITS-CLIP, high-throughput sequencing of RNAs isolated by cross-linking immunoprecipitation; IACUC, Institutional Animal Care and Use Committee; ICOS, inducible T-cell co-stimulator; IFNγ, interferon gamma; IL, interleukin; KO, knockout; LR, likelihood ratio; miRNA, microRNA; PD-1, programmed death-1; PMA, phorbol 12-myristate 13-acetate; pStat1, phosphorylated Stat1; pT_{reg}, peripheral Treg; qCML, quantile-adjusted conditional maximum likelihood; QLF, quasi-likelihood F; RBC, red blood cell; RIN, RNA integrity number; RNA-seq, RNA sequencing; SP, single positive; T_{conv}, conventional T; TCR, T cell receptor; T_{eff}, T effector; Th1, T helper cell 1; T_{reg}, regulatory T; TMM, trimmed mean of M values; VHL, von Hippel–Lindau; WT, wild-type; YFP, yellow fluorescent protein.

(TCR) avidity toward self-antigens. In contrast, peripheral T_{reg} (pT_{reg}) cells arise from naive $CD4^+$ T cells upon encounter of non–self-antigens in the context of appropriate cytokine stimulation [8–10]. Harnessing the power of T_{reg} cells to control immunological responses has a great potential for human therapy because, on one hand, T_{reg} cells can promote transplantation tolerance, but on the other, can hinder antitumor immunity.

Posttranscriptional regulation of gene expression by microRNA (miRNA), a class of small (approximately 22 nucleotides) noncoding RNA, recently emerged as a critical genetic element that is essential for T_{reg} cell function. T_{reg} cell–specific knockouts (KOs) of either *Drosha* or *Dicer* genes, encoding 2 endonucleases required for mature miRNA generation from precursor transcripts, phenocopy mice with *Foxp3* ablation, and develop severe systemic autoimmunity because of a defect in T_{reg} cell activity [11–13]. Furthermore, deletion of *Dicer* at the double positive (DP) thymocyte stage in mice significantly diminished the frequency of tT_{reg} cells, suggesting that miRNA-dependent gene control is also required for normal development of T_{reg} cells [11]. Thus, the current pressing challenge in the field is to determine how specific miRNA gene(s) exert control of the T_{reg} cell genetic program. The present report addresses this goal by examining the role of *miR-142* in T_{reg} cell development and function.

miR-142 is predominantly expressed in cells of hematopoietic origin and encodes 2 abundant mature miRNA molecules—miR-142-5p and miR-142-3p—which arise from the opposite strands of the hairpin-like miR-142 precursor. Using genetic loss-of-function studies, *miR-142* was previously implicated in the regulation of ontogenesis and function of several immune cell types. Our earlier report determined that deletion of this miRNA gene in mice results in aberrant B lymphopoiesis and impaired humoral immunity [14]. In addition, *miR-142*–deficient mice develop thrombocytopenia stemming from defective megakaryocyte maturation [15] and exhibit dysregulation of dendritic cell (DC) function [16]. Disruption of 2 *miR-142* paralog genes in zebra danio using zinc-finger nucleases was reported to cause aberrant neutrophil differentiation [17]. In the T-cell compartment, *miR-142* is required for the homeostasis of peripheral T effector (T_{eff}) cells, but is apparently dispensable for conventional T (T_{conv}) cell development in the thymus [14,18,19]. A recent study by Anandagoda and colleagues has demonstrated that *miR-142* is essential for the immunosuppressive activity of T_{reg} cells, but failed to reveal a significant role for this miRNA in T_{reg} cell development and homeostasis [20]. The authors suggest that posttranscriptional repression of the cAMP-hydrolyzing enzyme *Pde3b* by miR-142-5p isoform plays a key role in the regulation of the T_{reg} cell suppressive function.

Here, we show that mice with a conditional deletion of *miR-142* in T_{reg} cells develop severe autoimmune disease due to a profound defect in T_{reg} cell homeostasis and function. In addition, our findings suggest that *miR-142* plays an important role in tT_{reg} cell development. We have determined that the miR-142-3p isoform and its capacity to silence multiple interferon gamma (IFNγ)-associated genes play a critical role in mediating the regulatory activity of *miR-142* in T_{reg} cells. Global ablation of IFNγ rescues the T_{reg} cell defect and autoimmunity in $Foxp3^{Cre}miR\text{-}142^{fl/fl}$ mice, thus providing further evidence for the essential role of the *miR-142*-IFNγ signaling pathway in the regulation of T_{reg} cell homeostasis and function.

Results

miR-142 is dynamically expressed in T cells, and its global ablation results in a T_{reg} cell defect

Our efforts to define the role of *miR-142* in the regulation of T-cell tolerance stem from an unexpected observation that global *miR-142* ablation results in a marked T_{reg} cell defect. We found that germline *miR-142* KO mice display a significant drop in T_{reg} cell numbers in both

thymus and secondary lymphoid organs (S1A–S1C Fig), indicating that *miR-142* plays an important role in T_{reg} cell development and homeostasis. The observed defect was specific to T_{reg} cells, because thymic development of T_{conv} cells was largely normal in the germline *miR-142* KO mice [14,18,19]. Our expression profiling experiments revealed that the mature miR-142-3p isoform is abundantly expressed in thymic and pT_{reg} cells, whereas the mature miR-142-5p isoform is present in significantly lower amounts (S1D Fig). The level of miR-142-3p expression in T_{reg} cells is roughly comparable to the expression of this miRNA in naive and activated T_{eff} cells. Of note, *miR-142* is dynamically expressed during T-cell development: its abundance gradually increases following T-cell maturation in the thymus and reaches a peak at the single positive (SP) thymocyte stage; however, mature T cells that egress from the thymus into periphery display a somewhat reduced *miR-142* expression in comparison to SP thymocytes (S1D Fig).

Lethal autoimmune disease in mice with T_{reg} cell–specific *miR-142* deletion

To determine the role of *miR-142* in T_{reg} cell function, we created mice with a T_{reg} cell–specific ablation of this miRNA (hereafter *Foxp3*^{Cre}*miR-142*$^{fl/fl}$ mice). *Foxp3*^{Cre} deleter/reporter mice [21] that were used to generate the T_{reg} cell–specific excision of *miR-142* conditional allele (*miR-142*$^{fl/fl}$) express Cre recombinase as a fusion protein with yellow fluorescent protein (YFP) under the control of endogenous *Foxp3* promoter, providing an effective way to purify T_{reg} cells by flow cytometry. As expected, $CD4^+YFP^+$ T_{reg} cells isolated from *Foxp3*^{Cre}*miR-142*$^{fl/fl}$ mice were virtually devoid of mature miR-142-3p, whereas expression of this miRNA in $CD4^+$ T_{conv} cells remained unchanged (S1E Fig). Despite appearing normal at birth, *Foxp3*^{Cre}*miR-142*$^{fl/fl}$ mice exhibited an apparent failure to thrive: they had a very short life span (Fig 1A), were smaller in size (Fig 1B), and had significantly lower body weight than wild-type (WT; *Foxp3*^{Cre}) littermates (Fig 1C). Gross morphological analysis revealed that *Foxp3*^{Cre}*miR-142*$^{fl/fl}$ mice developed a systemic lymphoproliferative autoimmune disorder that was characterized by significant lymphadenopathy (Fig 1D and S1J Fig), mild splenomegaly (Fig 1D, S1F and S1H Fig), thymic involution (S1G and S1I Fig), dermatitis (Fig 1B), and massive immune cell infiltration into various peripheral organs (Fig 1E). Taken together, the phenotypic findings from *Foxp3*^{Cre}*miR-142*$^{fl/fl}$ mice resemble the autoimmune pathology observed in mice with severe T_{reg} cell defects (e.g., *scurfy* mutants or *Foxp3* KO mice [3–7]), suggesting that *miR-142* is involved in the regulation of T_{reg} cell homeostasis or stability.

T_{reg} cell defect and aberrant T-cell activation in *Foxp3*^{Cre}*miR-142*$^{fl/fl}$ mice

In agreement with this notion, we observed a marked reduction in T_{reg} cell population in the *Foxp3*^{Cre}*miR-142*$^{fl/fl}$ spleen (Fig 2A). Furthermore, the absolute number of thymic T_{reg} cells in *Foxp3*^{Cre}*miR-142*$^{fl/fl}$ mice was also significantly lower, despite a slight increase in the frequency of T_{reg} cells in the atrophied thymus (S2A and S2B Fig). Because T_{reg} cells play a crucial role in suppressing self-destructive responses elicited by autoreactive T cells, we examined the activation status of peripheral T cells in *Foxp3*^{Cre}*miR-142*$^{fl/fl}$ mice by flow cytometry. In comparison to WT mice, the number of $CD4^+$ and $CD8^+$ T cells with memory/effector phenotype ($CD44^{hi}CD62L^{lo}$) was significantly higher in the spleen and lymph nodes of *Foxp3*^{Cre}*miR-142*$^{fl/fl}$ mice, whereas the pool of naive ($CD44^{lo}CD62L^{hi}$) $CD4^+$ and $CD8^+$ T cells in the KO animals diminished considerably (Fig 2B and 2C, S2C and S2D Fig). *Foxp3*^{Cre}*miR-142*$^{fl/fl}$ mice exhibited an expansion of peripheral $CD4^+$ and $CD8^+$ T-cell compartments (S2G Fig), most likely due to a failure of *miR-142*–deficient T_{reg} cells to suppress proliferation of hyperactivated T lymphocytes. In addition, both $CD4^+$ and $CD8^+$ T cells isolated from *Foxp3*^{Cre}*miR-142*$^{fl/fl}$ mice displayed a sharp increase in production of IFNγ (Fig 2D and 2E, S2E and S2F Fig), a

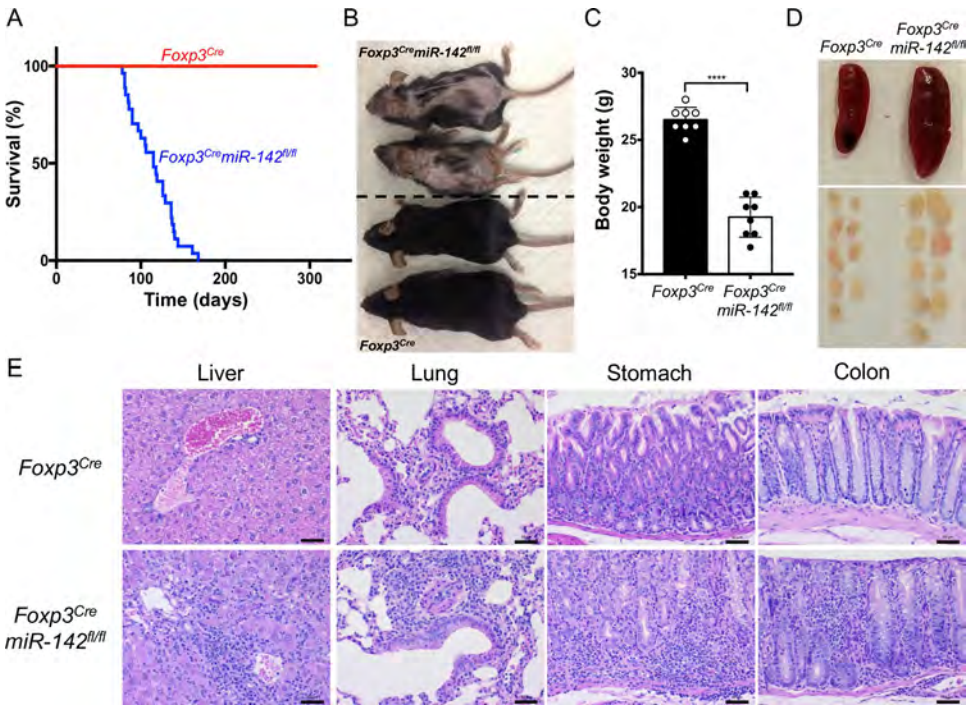

Fig 1. Fatal autoimmune disorder in mice with T_{reg} cell–specific disruption of *miR-142*. (**A**) Kaplan–Meier survival curves of *Foxp3*^{Cre} and *Foxp3*^{Cre}*miR-142*$^{fl/fl}$ mice ($n = 27$ per group) ($P < 0.0001$). (**B**) Photograph of 14-week-old female *Foxp3*^{Cre} (lower 2) and *Foxp3*^{Cre}*miR-142*$^{fl/fl}$ (upper 2) mice. Note smaller body size and severe dermatitis in *Foxp3*^{Cre}*miR-142*$^{fl/fl}$ mice. (**C**) Body weight comparison of 8- to 10-week-old male *Foxp3*^{Cre} and *Foxp3*^{Cre}*miR-142*$^{fl/fl}$ mice ($n = 8$ per group). (**D**) Representative images of spleen and peripheral lymph nodes from *Foxp3*^{Cre} (left) and *Foxp3*^{Cre}*miR-142*$^{fl/fl}$ (right) mice. (**E**) HE staining of liver, lung, stomach, and colon tissue sections from *Foxp3*^{Cre} and *Foxp3*^{Cre}*miR-142*$^{fl/fl}$ mice. Note massive accumulation of leukocytes in *Foxp3*^{Cre}*miR-142*$^{fl/fl}$ tissues. Scale bar, 50 μm. Results are shown as mean ± SD. *P* values were determined by log-rank test (A) or 2-tailed Student *t* test (C); ****, $P < 0.0001$. The underlying raw data can be found in S1 Data file. HE, hematoxylin–eosin; SD, standard deviation; T_{reg}, regulatory T.

https://doi.org/10.1371/journal.pbio.3001552.g001

pro-inflammatory cytokine that promotes type 1 T helper cell 1 (Th1) responses. In contrast, no obvious changes in interleukin (IL)-4 (secreted by Th2 cells) or IL-17 (secreted by Th17 cells) production by splenic CD4$^+$ T cells were observed in *Foxp3*^{Cre}*miR-142*$^{fl/fl}$ animals (S2H Fig). Thus, our findings suggest that conditional *miR-142* deletion impairs T_{reg} cell function and subsequently drives severe dysregulation of T_{eff} responses.

miR-142 is essential for the homeostasis and suppressive activity of T_{reg} cells

To determine how *miR-142* ablation affects suppressive function of T_{reg} cells, we cocultured purified *miR-142*–deficient and *miR-142*–sufficient T_{reg} cells together with WT T_{conv} cells that were induced to proliferate by antigen receptor stimulation. We found that *miR-142*–deficient T_{reg} cells exhibited a comparable capacity to restrain the proliferation of activated T_{conv} cells as *miR-142*–sufficient T_{reg} cells in this classical *in vitro* T_{reg} cell suppression assay (Fig 3A, S3A Fig). Similar *in vitro* findings were previously reported for *miR-146a* and *miR-181a/b-1*, two other miRNAs that are implicated in the regulation of T_{reg} cell activity [22,23]. Nevertheless, adoptive transfer of *miR-142*–deficient T_{reg} cells failed to attenuate development of systemic inflammatory syndrome in a mouse model of acute graft-versus-host disease (aGVHD). Lethally irradiated *BALB/c* mice (H2^d) transplanted with allogeneic CD4$^+$ T_{conv} cells from

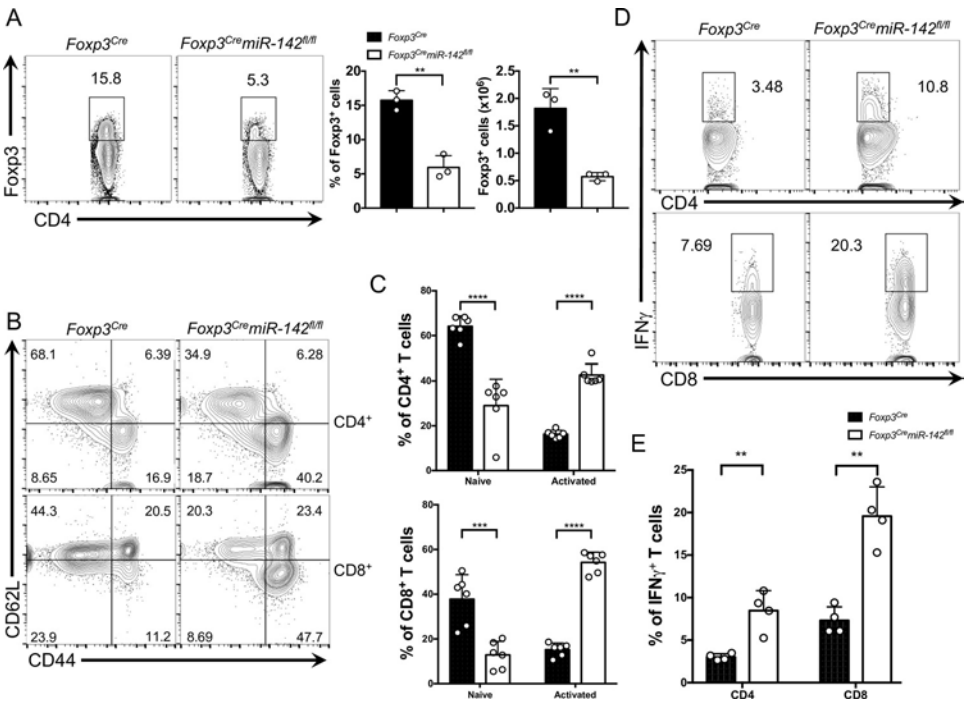

Fig 2. *miR-142* is required for maintenance of T_{reg} cell–mediated immune tolerance. (**A**) Left panel, FACS analysis of splenic lymphocytes from 12-week-old *Foxp3*^{Cre} and *Foxp3*^{Cre}*miR-142*$^{fl/fl}$ mice with anti-CD4 and anti-Foxp3 specific antibodies. Numbers indicate percentage of CD4$^+$Foxp3$^+$ T_{reg} cells in the gate. Right panel, frequency and absolute number of T_{reg} cells in *Foxp3*^{Cre} and *Foxp3*^{Cre}*miR-142*$^{fl/fl}$ spleens ($n = 3$ per group). (**B**) FACS analysis of splenic CD4$^+$ and CD8$^+$ T cells from 8- to 10-week-old *Foxp3*^{Cre} and *Foxp3*^{Cre}*miR-142*$^{fl/fl}$ mice with anti-CD44 and anti-CD62L specific antibodies. Numbers indicate percentage of cells in the quadrants. (**C**) Frequency of naive (CD44$^-$CD62L$^+$) and activated (CD44$^+$CD62L$^-$) splenic CD4$^+$ (top) and CD8$^+$ (bottom) T lymphocytes isolated from 8- to 10-week-old *Foxp3*^{Cre} and *Foxp3*^{Cre}*miR-142*$^{fl/fl}$ mice ($n = 6$ per group). (**D**) Intracellular FACS analysis of IFNγ production in splenic CD4$^+$ (top) and CD8$^+$ (bottom) T cells. Numbers indicate percentage of IFNγ$^+$ T cells in the gate. (**E**) Frequency of IFNγ expressing splenic CD4$^+$ and CD8$^+$ T cells isolated from 8- to 10-week-old *Foxp3*^{Cre} and *Foxp3*^{Cre}*miR-142*$^{fl/fl}$ mice ($n = 4$ per group). Results are shown as mean ± SD. *P* values were calculated using 2-tailed Student *t* test. **, $P < 0.01$; ***, $P < 0.001$; ****, $P < 0.0001$. The underlying numerical raw data can be found in S1 Data file. The underlying flow cytometry raw data can be found at the Figshare repository. FACS, fluorescence activated cell sorting; IFNγ, interferon gamma; SD, standard deviation; T_{reg}, regulatory T.

https://doi.org/10.1371/journal.pbio.3001552.g002

C57BL/6 donors (H2^b) rapidly developed sublethal aGVHD that was manifested by hunched posture, severe diarrhea, and significant weight loss in the host mice (Fig 3B and 3C). The concomitant transfer of WT T_{reg} cells together with allogeneic donor T cells reduced the severity of aGVHD symptoms, as indicated by diminished diarrhea and less pronounced body weight loss in the host mice (Fig 3C). In contrast, adoptive transfer of *miR-142*–deficient T_{reg} cells failed to protect the host mice from the development of aGVHD and resulted in mortality, perhaps by exacerbating the inflammatory response (Fig 3B and 3C). The failure of *miR-142*–deficient T_{reg} cells to suppress aGVHD indicated an essential role of *miR-142* in the regulation of T_{reg} cell suppressive activity *in vivo*. In addition, a significantly lower frequency of donor *miR-142*–deficient T_{reg} cells in the spleens of host mice 17 days posttransplantation (Fig 3D) suggested the survival or homeostatic defect of *miR-142*–deficient T_{reg} cells.

To test whether *miR-142* ablation affects survival of T_{reg} cells, we compared induction of apoptosis in *miR-142*–sufficient and *miR-142*–deficient T_{reg} cells in response to TCR stimulation. We found that purified splenic *miR-142* KO T_{reg} cells were more prone to activation-induced cell death (Fig 3E), although resting T_{reg} cells from *Foxp3*^{Cre}*miR-142*$^{fl/fl}$ spleen displayed no obvious difference in Annexin V staining (S3B Fig). To further establish the cell-

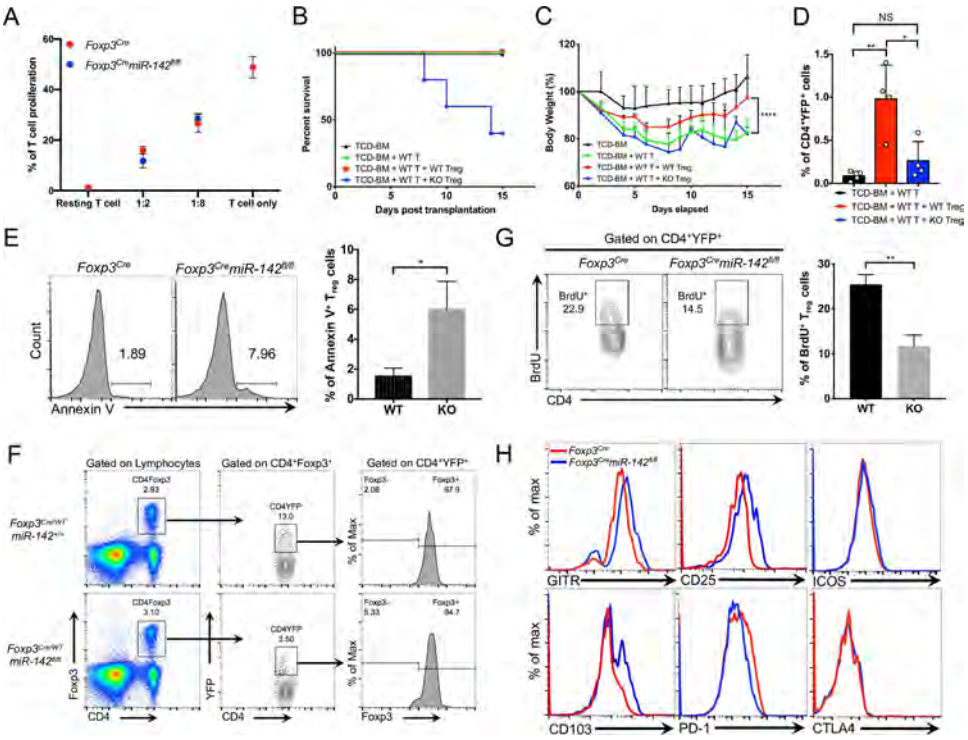

Fig 3. *miR-142* ablation impairs suppressive function and homeostasis of T_{reg} cells. (**A**) *in vitro* T_{reg} suppression assay. Purified $CD4^+$ T_{conv} cells were loaded with CTV dye and incubated with FACS-sorted T_{reg} cells from *Foxp3*^{Cre} (red dots) and *Foxp3*^{Cre}*miR-142*$^{fl/fl}$ (blue dots) spleens ($n = 3$) in the presence of beads coated with anti-CD3 and anti-CD28 specific antibodies. After 3 days, the rate of T_{conv} cell proliferation was determined by flow cytometry as dilution of the CTV dye. Several T_{reg} to T_{conv} cell ratios were analyzed as indicated in the graph. Unstimulated T_{conv} cells were used as control. (**B**) Survival of mice in aGVHD model. Lethally irradiated BALB/c recipient mice were transplanted with T-cell–depleted bone marrow from C57BL/6J mice (TCD-BM), $Thy1.2^+CD4^+$ T cells from C57BL/6J spleens (WT T), and $CD4^+YFP^+$ T_{reg} cells derived from either *Foxp3*^{Cre} (WT) or *Foxp3*^{Cre}*miR-142*$^{fl/fl}$ (KO) spleens ($P = 0.0096$; $n = 5$ per group). (**C**) Body weight analysis of mice in aGVHD model. Mouse grouping as in B ($n = 5$ per group). (**D**) Frequency of donor *Foxp3*^{Cre} (WT) or *Foxp3*^{Cre}*miR-142*$^{fl/fl}$ (KO) $CD4^+YFP^+$ T_{reg} cells in spleens of BALB/c recipient mice on day 17 after BMT ($n = 4$ for all groups). (**E**) Left panel, FACS analysis of activation-induced cell death in splenic *Foxp3*^{Cre} and *Foxp3*^{Cre}*miR-142*$^{fl/fl}$ T_{reg} cells. Apoptotic T_{reg} cells were detected by Annexin V staining upon stimulation with anti-CD3 (1 μg/ml) specific antibodies for 48 hours. Numbers indicate percentage of Annexin V^+ cells. Right panel, the frequency of Annexin V^+ *Foxp3*^{Cre} (WT) and *Foxp3*^{Cre}*miR-142*$^{fl/fl}$ (KO) T_{reg} cells ($n = 3$ per group). (**F**) FACS analysis of $CD4^+Foxp3^+$ T_{reg} cells (left panels), YFP-Cre expression in $CD4^+Foxp3^+$ T_{reg} cells (middle panels), and Foxp3 expression in $CD4^+YFP^+$ *miR-142*–sufficient and *miR-142*–deficient T_{reg} cells (right panels) from female *Foxp3*$^{Cre/WT}$*miR-142*$^{+/+}$ and *Foxp3*$^{Cre/WT}$*miR-142*$^{fl/fl}$ mice. (**G**) Left panel, intracellular FACS analysis of BrdU incorporation into T_{reg} cells isolated from *Foxp3*^{Cre} and *Foxp3*^{Cre}*miR-142*$^{fl/fl}$ spleens. FACS plots were pregated on $CD4^+YFP^+$ T_{reg} cells, and numbers indicate percentage of cells in the gate. Right panel, the frequency of $BrdU^+$ T_{reg} cells in *Foxp3*^{Cre} (WT) and *Foxp3*^{Cre}*miR-142*$^{fl/fl}$ (KO) spleens 16 hours after BrdU injection (1mg i.p.) ($n = 3$ per group). (**H**) FACS analysis of cell surface markers on T_{reg} cells isolated from *Foxp3*^{Cre} (red) and *Foxp3*^{Cre}*miR-142*$^{fl/fl}$ (blue) spleens with anti-GITR, anti-CD25, anti-CD103, anti-PD-1, anti-CTLA-4, and anti-ICOS specific antibodies. Histograms were pregated on $CD4^+YFP^+$ T_{reg} cells. Results are shown as mean ± SD. *P* values were calculated using log-rank test (B), 1-way ANOVA (C), and 2-tailed Student *t* test (D, E, G). *, $P < 0.05$; **, $P < 0.01$; ****, $P < 0.0001$; NS, not significant. The underlying numerical raw data can be found in S1 Data file. The underlying flow cytometry raw data can be found at the Figshare repository. aGVHD, acute graft-versus-host disease; BMT, bone marrow transplantation; CTV, cell trace violet; FACS, fluorescence activated cell sorting; KO, knockout; SD, standard deviation; T_{reg}, regulatory T; YFP, yellow fluorescent protein; WT, wild-type.

https://doi.org/10.1371/journal.pbio.3001552.g003

intrinsic role of *miR-142* in T_{reg} cell homeostasis, we enumerated *miR-142*–deficient T_{reg} cells in *Foxp3*$^{Cre/WT}$*miR-142*$^{fl/fl}$ heterozygous female mice. Due to random X chromosome inactivation of *Foxp3*^{Cre} allele, female *Foxp3*$^{Cre/WT}$*miR-142*$^{fl/fl}$ mice generate both YFP^- *miR-142*–sufficient and YFP^+ *miR-142*–deficient T_{reg} cells. Our analysis revealed a marked reduction in the

frequency of splenic YFP$^+$ *miR-142*–deficient T_{reg} cells in the mosaic mice (Fig 3F, S3C Fig), indicating that *miR-142* plays a cell-autonomous role in T_{reg} cell homeostasis. In addition, *in vivo* labeling experiments using 5-bromo-2-deoxyuridine (BrdU) revealed that *miR-142*–deficient T_{reg} cells have almost 2-fold lower proliferation capacity than WT T_{reg} cells (Fig 3G). Collectively, these findings implicate *miR-142* in the regulation of homeostatic maintenance and proliferation of T_{reg} cells.

Analysis of cell surface markers on pT_{reg} cells from *Foxp3^{Cre}miR-142$^{fl/fl}$* mice by flow cytometry suggested that *miR-142*–deficient T_{reg} cells display an activated/effector phenotype [24]. Consistent with this notion, *miR-142*–deficient T_{reg} cells exhibited an up-regulation of several T-cell activation markers, including glucocorticoid-induced tumor necrosis factor receptor family-related gene (GITR), interleukin-2 receptor α (CD25), and integrin α_E (CD103) (Fig 3H, S3D Fig). On the other hand, the levels of programmed death-1 (PD-1) receptor, which protects T_{reg} cells from apoptosis [25], were significantly lower on *miR-142*–deficient T_{reg} cells (Fig 3H, S3D Fig), although expression of other immune checkpoint molecules such as cytotoxic T-lymphocyte associated protein 4 (CTLA4) and inducible T-cell co-stimulator (ICOS) was not affected.

Specific deletion of *miR-142* in T_{reg} cells results in global derepression of miR-142-3p targets

To uncover the molecular mechanism by which *miR-142* controls T_{reg} cell function, we performed global transcriptome analysis of splenic CD4$^+$YFP$^+$ *miR-142*–sufficient and *miR-142*–deficient T_{reg} cells using RNA sequencing (RNA-seq). We identified a total of 1,520 genes showing statistically significant change in expression due to *miR-142* ablation, 988 of which were up-regulated and 532 of which were down-regulated in *miR-142*–deficient T_{reg} cells (Fig 4A, S1 Table). Analysis of differentially expressed genes in *miR-142*–deficient T_{reg} cells with the SylArray and ToppFun software algorithms [26,27] revealed a significant enrichment of miR-142-3p (85 out of 429 annotated target genes), but not miR-142-5p, direct targets among the up-regulated genes (Fig 4B), suggesting that impaired homeostasis and function of T_{reg} cells in *Foxp3^{Cre}miR-142$^{fl/fl}$* mice are most likely driven by the loss of mature miR-142-3p expression. This conclusion aligns well with significantly more abundant expression of miR-142-3p in T_{reg} cells (S1D Fig) and a large number of previously published observations from a broad spectrum of *miR-142*–deficient immune cell types [14–18,28–30]. Nevertheless, the possibility that miR-142-5p contributes to the regulation of T_{reg} cell biology (as was recently proposed by Anandagoda and colleagues [20]) either by controlling the expression of a limited number of target mRNAs or by exerting its regulatory effect entirely at the translational level cannot be excluded, although our results suggest that the T_{reg} cell defect in *Foxp3^{Cre}miR-142$^{fl/fl}$* mice is primarily mediated by miR-142-3p.

Pathway enrichment analysis of the differentially expressed genes identified significant overrepresentation of biological processes that are associated with innate and adaptive immune responses (S2 Table). In line with these findings, *miR-142*–deficient T_{reg} cells display an up-regulated expression of diverse cytokine, chemokine, and immune receptor genes (S4A Fig). One potential caveat of this finding is that the aberrant inflammation observed in *Foxp3^{Cre}miR-142$^{fl/fl}$* mice can conceivably induce pro-inflammatory changes in the gene expression of T_{reg} cells. In addition, expression of several T_{reg} cell signature genes was altered by the loss of *miR-142* (S4B Fig). Interestingly, the transcripts up-regulated in *miR-142*–deficient T_{reg} cells were enriched for genes from the IFNγ signaling network according to the Enrichr software algorithm [31] and the Gene Set Enrichment Analysis (GSEA) [32] (Fig 4C, S4C Fig, S2 Table). In agreement with our bioinformatic findings, we found that *miR-142*–deficient T_{reg} cells produced significantly more IFNγ in comparison with WT cells (Fig 4D and 4E,

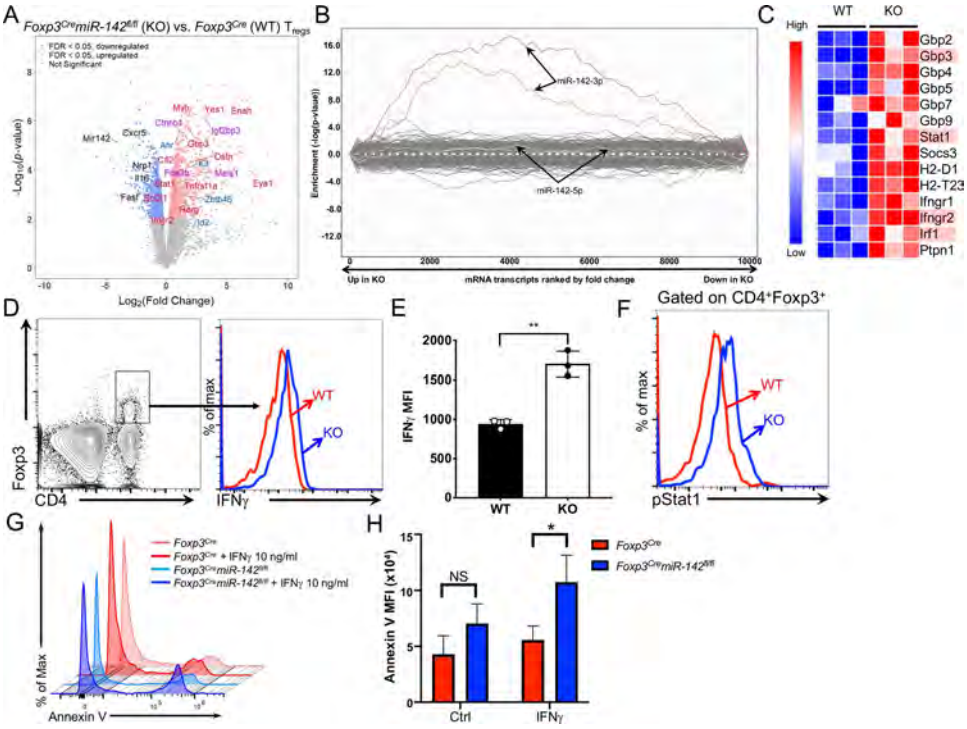

Fig 4. Global derepression of miR-142-3p targets and dysregulated IFNγ signaling in *miR-142*–deficient T_{reg} cells. (**A**) Volcano plot showing statistical significance versus magnitude of change for visualizing the distribution of differentially expressed genes. Selected *miR-142* targets (red for -3p, blue for -5p, and purple for both) and other genes of functional interest (black; including *miR-142*) are labeled. (**B**) Global derepression of miR-142-3p target genes in *miR-142*–deficient T_{reg} cells. SylArray analysis of 3′ UTRs of differentially expressed transcripts in *miR-142*–deficient T_{reg} cells for miRNA SCSs. Enrichment *P* values for each miRNA SCS are plotted on the y-axis against the ranked gene list on the x-axis (the most up-regulated genes in *miR-142*–deficient T_{reg} cells are toward the left, while the most down-regulated genes are toward the right). Plots corresponding to two 7-mer seeds of miR-142-3p are highlighted in red and orange, and two 7-mer seeds of miR-142-5p are depicted in green and yellow. (**C**) Heat map of expression profiles of IFNγ-associated genes in $Foxp3^{Cre}$ (WT) and $Foxp3^{Cre}miR\text{-}142^{fl/fl}$ (KO) T_{reg} cells ($n = 3$ per group). Genes highlighted in red are putative targets of miR-142-3p. (**D–F**) Intracellular FACS analysis of IFNγ production (**D**) and Stat1(Y701) phosphorylation (**F**) in $Foxp3^{Cre}$ (red line) and $Foxp3^{Cre}miR\text{-}142^{fl/fl}$ (blue line) $CD4^+Foxp3^+$ T_{reg} cells. (**E**) MFI of IFNγ expression in $Foxp3^{Cre}$ (WT) and $Foxp3^{Cre}miR\text{-}142^{fl/fl}$ (KO) T_{reg} cells ($n = 3$ per group). (**G**) FACS analysis of Annexin V-stained splenic $CD4^+YFP^+$ T_{reg} cells from $Foxp3^{Cre}$ (WT) or $Foxp3^{Cre}miR\text{-}142^{fl/fl}$ (KO) mice. Splenocytes were incubated for 24 hours in cell culture in the presence or absence of IFNγ (10 ng/ml) prior to flow cytometry analysis. (**H**) MFI of Annexin V staining on T_{reg} cells from $Foxp3^{Cre}$ (WT) *or* $Foxp3^{Cre}miR\text{-}142^{fl/fl}$ (KO) spleens with or without IFNγ treatment (10 ng/ml). Results are shown as mean ± SD. *P* values were calculated using 2-tailed Student t test. *, $P < 0.05$; **, $P < 0.01$; NS, not significant. The underlying numerical raw data can be found in S1 Table and S1 Data file. The underlying flow cytometry raw data can be found at the Figshare repository. FACS, fluorescence activated cell sorting; IFNγ, interferon gamma; KO, knockout; MFI, mean fluorescence intensity; SCS, seed complementary sequence; SD, standard deviation; T_{reg}, regulatory T; WT, wild-type.

https://doi.org/10.1371/journal.pbio.3001552.g004

S4D Fig) and displayed dysregulation of IFNγ signaling, manifested by a substantial increase in Stat1 activation (Fig 4F, S4E Fig). Because *miR-142* deletion impairs T_{reg} cell homeostasis, we examined the effect of IFNγ stimulation on T_{reg} cell survival and found that IFNγ treatment significantly enhanced apoptosis of *miR-142*–deficient T_{reg} cells *in vitro* (Fig 4G and 4H).

Ifng ablation rescues the T_{reg} homeostatic defect and alleviates development of the systemic autoimmune disorder in $Foxp3^{Cre}miR\text{-}142^{fl/fl}$ mice

To determine how dysregulated IFNγ signaling impacts the homeostasis of *miR-142*–deficient T_{reg} cells, we generated $Foxp3^{Cre}miR\text{-}142^{fl/fl}Ifng^{-/-}$ double KO mice by crossing $Foxp3^{Cre}miR\text{-}$

142$^{fl/fl}$ mice with *Ifng*$^{-/-}$ mice. Intriguingly, our analysis revealed a complete rescue of the T_{reg} homeostatic defect in the double KO mice (Fig 5A). Furthermore, *Ifng* deletion alleviated development of the systemic lymphoproliferative and fatal autoimmune disease in *Foxp3*^{Cre}*miR-142*$^{fl/fl}$ mice. This conclusion was supported by observations of improved survival (Fig 5B), body weight normalization (Fig 5C) and marked rescue of the lymphadenopathy (Fig 5D), splenomegaly (Fig 5D and 5E), and thymic involution (Fig 5F) defects in *Foxp3*^{Cre}*miR-142*$^{fl/fl}$*Ifng*$^{-/-}$ mice. Of note, the double KO mice displayed an abatement of tissue inflammation, evidenced by a significant decrease in the amount of immune cell infiltration into peripheral tissues (Fig 5G). These

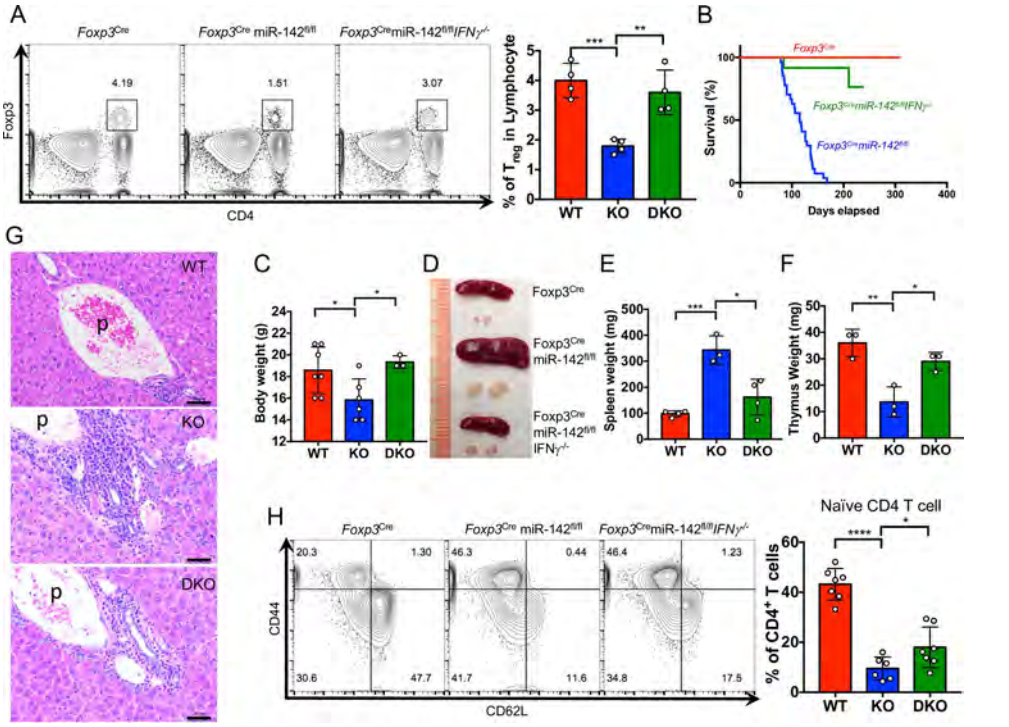

Fig 5. Blockade of IFNγ production rescues the T_{reg} cell homeostatic defect and alleviates systemic autoimmunity in *Foxp3*^{Cre}*miR-142*$^{fl/fl}$ mice. (**A**) Left panel, FACS analysis of splenic T_{reg} cells from 12- to 15-week-old *Foxp3*^{Cre} (WT), *Foxp3*^{Cre}*miR-142*$^{fl/fl}$ (KO), and *Foxp3*^{Cre}*miR-142*$^{fl/fl}$*Ifng*$^{-/-}$ (DKO) mice ($n = 4$ per group). Foxp3^{+}CD4^{+} T_{reg} cells are gated and numbers indicate the percentage of cells in the gate. Right panel, frequency of CD4^{+}Foxp3^{+} T_{reg} cells in *Foxp3*^{Cre} (WT), *Foxp3*^{Cre}*miR-142*$^{fl/fl}$ (KO), and *Foxp3*^{Cre}*miR-142*$^{fl/fl}$*Ifng*$^{-/-}$ (DKO) spleens. (**B**) Kaplan–Meier survival curves for *Foxp3*^{Cre} (red line; $n = 27$), *Foxp3*^{Cre}*miR-142*$^{fl/fl}$ (blue line; $n = 27$), and *Foxp3*^{Cre}*miR-142*$^{fl/fl}$*Ifng*$^{-/-}$ (green line; $n = 12$) mice. (**C**) Body weight comparison of 7- to 9-week-old female *Foxp3*^{Cre} (WT, red bar, $n = 7$), *Foxp3*^{Cre}*miR-142*$^{fl/fl}$ (KO, blue bar, $n = 6$), and *Foxp3*^{Cre}*miR-142*$^{fl/fl}$*Ifng*$^{-/-}$ (DKO, green bar, $n = 3$) mice. (**D**) Representative images of spleen and inguinal lymph nodes from 14-week-old *Foxp3*^{Cre}, *Foxp3*^{Cre}*miR-142*$^{fl/fl}$, and *Foxp3*^{Cre}*miR-142*$^{fl/fl}$*Ifng*$^{-/-}$ mice. (**E**) Spleen weights in 12- to 15-week-old *Foxp3*^{Cre} (WT, red bar, $n = 4$), *Foxp3*^{Cre}*miR-142*$^{fl/fl}$ (KO, blue bar, $n = 3$), and *Foxp3*^{Cre}*miR-142*$^{fl/fl}$*Ifng*$^{-/-}$ (DKO, green bar, $n = 4$) mice. (**F**) Thymus weights (1 lobe) in 6- to 8-week-old *Foxp3*^{Cre} (WT, red bar), *Foxp3*^{Cre}*miR-142*$^{fl/fl}$ (KO, blue bar), and *Foxp3*^{Cre}*miR-142*$^{fl/fl}$*Ifng*$^{-/-}$ (DKO, green bar) mice ($n = 3$ per group). (**G**) HE staining of liver tissue sections from *Foxp3*^{Cre} (WT), *Foxp3*^{Cre}*miR-142*$^{fl/fl}$ (KO), and *Foxp3*^{Cre}*miR-142*$^{fl/fl}$*Ifng*$^{-/-}$ (DKO) mice. Note diminished infiltration of leukocytes into liver tissue around portal vein area in DKO mice. Scale bar, 50 μm; p, portal vein. (**H**) Left panel, FACS analysis of CD44 and CD62L expression in splenic CD4^{+} T cells from 7- to 15-week-old *Foxp3*^{Cre}, *Foxp3*^{Cre}*miR-142*$^{fl/fl}$, and *Foxp3*^{Cre}*miR-142*$^{fl/fl}$*Ifng*$^{-/-}$ mice. Numbers indicate percentage of cells in the quadrants. Right panel, frequency of CD44^{-}CD62L^{+} naive CD4^{+} T cell in *Foxp3*^{Cre} (WT, $n = 7$), *Foxp3*^{Cre}*miR-142*$^{fl/fl}$ (KO, $n = 6$), and *Foxp3*^{Cre}*miR-142*$^{fl/fl}$*Ifng*$^{-/-}$ (DKO, $n = 7$) spleens. Results are shown as mean ± SD. *P* values were calculated using 2-tailed Student *t* test. *, $P < 0.05$; **, $P < 0.01$; ***, $P < 0.001$; ****, $P < 0.0001$. WT, *Foxp3*^{Cre}; KO, *Foxp3*^{Cre}*miR-142*$^{fl/fl}$; DKO, *Foxp3*^{Cre}*miR-142*$^{fl/fl}$*Ifng*$^{-/-}$. The underlying numerical raw data can be found in S1 Data file. The underlying flow cytometry raw data can be found at the Figshare repository. DKO, double knockout; FACS, fluorescence activated cell sorting; HE, hematoxylin–eosin; IFNγ, interferon gamma; KO, knockout; SD, standard deviation; WT, wild-type.

https://doi.org/10.1371/journal.pbio.3001552.g005

morphological changes correlated with a modest increase in the number of naive T_{conv} cells in the periphery of *Foxp3*^{Cre}*miR-142*$^{fl/fl}$*Ifng*$^{-/-}$ mice (Fig 5H), suggesting that the *miR-142*-IFNγ signaling axis is primarily important for maintaining T_{reg} cell homeostasis. Despite the restoration of T_{reg} cell frequency in *Foxp3*^{Cre}*miR-142*$^{fl/fl}$*Ifng*$^{-/-}$ mice, the remaining hyperactivation of $CD4^+$ T_{conv} cells in the double KO mice implies a potential role for *miR-142* in the regulation of T_{reg} cell immunosuppressive activity.

miR-142-3p targets multiple IFNγ-associated genes

Several of the IFNγ-associated genes that were derepressed in *miR-142*–deficient T_{reg} cells, including *Ifngr2*, *Stat1*, *Irf1*, and *Gbp3*, are predicted by the TargetScan algorithm [33] as putative direct targets of miR-142-3p (Fig 4C, S5A Fig). We validated these bioinformatic predictions by examining the high-throughput sequencing of RNAs isolated by cross-linking immunoprecipitation (HITS-CLIP) database that was previously compiled by Rudensky and colleagues [34]. In activated $CD4^+$ T cells, 2 of the 4 (*Ifngr2* and *Gbp3)* target genes showed detectible peaks of Ago2 binding activity in their respective 3′ UTRs, corresponding to predicted binding sites for miR-142-3p (S5A Fig). An extended analysis of the HITS-CLIP database revealed hypoxia-induced factor 1 alpha (*Hif1a*) as a potential miR-142-3p target (Fig 6A). Our interest in this transcription factor was prompted by a previous report that implicated *Hif1a* in the regulation of T_{reg} cell homeostasis and suppressive function through the control of IFNγ expression [35]. Using 3′ UTR luciferase reporter assay, we confirmed the capacity of miR-142-3p to attenuate *Hif1a and Ifngr2* expression by binding directly to evolutionary conserved seed sequences in their respective 3′ UTRs (Fig 6B, S5B Fig). In line with these findings, we detected a significant increase in Hif1α and IFNγR2 protein levels in *miR-142*–deficient T_{reg} cells, whereas Hif1α expression in $CD4^+$ T_{conv} cells remained unchanged (Fig 6C, S5C and S5D Fig). Of note, we did not observe changes in *Hif1a* mRNA expression in T_{reg} cells lacking *miR-142* expression.

In addition, we examined the capacity of miR-142-3p to regulate the expression of phosphodiesterase 3b (*Pde3b*), which was recently identified as a critical miR-142-5p target gene modulating T_{reg} cell activity [20]. In agreement with the previously published results, we detected an approximately 3-fold increase of *Pde3b* mRNA expression in *miR-142*–deficient T_{reg} cells (S1 Table). Analysis of the *Pde3b* 3′ UTR by the TargetScan algorithm revealed 2 putative poorly conserved miR-142-5p binding sites and a single predicted poorly conserved miR-142-3p binding site (S5E Fig). Using the 3′ UTR luciferase reporter assay, we determined that overexpression of *miR-142* precursor can modestly attenuate *Pde3b* expression. Interestingly, we observed that mutation of the miR-142-3p binding site in the *Pde3b* 3′ UTR can completely negate the silencing effect of *miR-142* on the *Pde3b* reporter (S5B and S5F Fig). Thus, our findings have uncovered *Pde3b* as a novel miR-142-3p target gene, providing additional evidence for the critical role of miR-142-3p isoform in the regulation of T_{reg} cell biology.

Hif1a haploinsufficiency partially rescues the T_{reg} cell homeostasis defect in *Foxp3*^{Cre}*miR-142*$^{fl/fl}$ mice

Next, we sought to determine the contribution of the *miR-142-Hif1a* axis in T_{reg} cell homeostasis and function. We lowered the *Hif1a* gene dose in *miR-142*–deficient T_{reg} cells by crossing *Foxp3*^{Cre}*miR-142*$^{fl/fl}$ mice with mice carrying a conditional *Hif1a* allele (*Hif1a*$^{fl/fl}$). The resultant *Foxp3*^{Cre}*miR-142*$^{fl/fl}$*Hif1a*$^{+/fl}$ mice expressed normal levels of Hif1α protein in T_{reg} cells (S6A Fig) and displayed a partial rescue of T_{reg} cell abundance (Fig 6D, S6B Fig). Furthermore, *Foxp3*^{Cre}*miR-142*$^{fl/fl}$*Hif1a*$^{+/fl}$ mice exhibited a partial reduction in the frequency of activated/effector $CD4^+$ T cells in the periphery (Fig 6E and 6F). Nevertheless, *Hif1a* haploinsufficiency

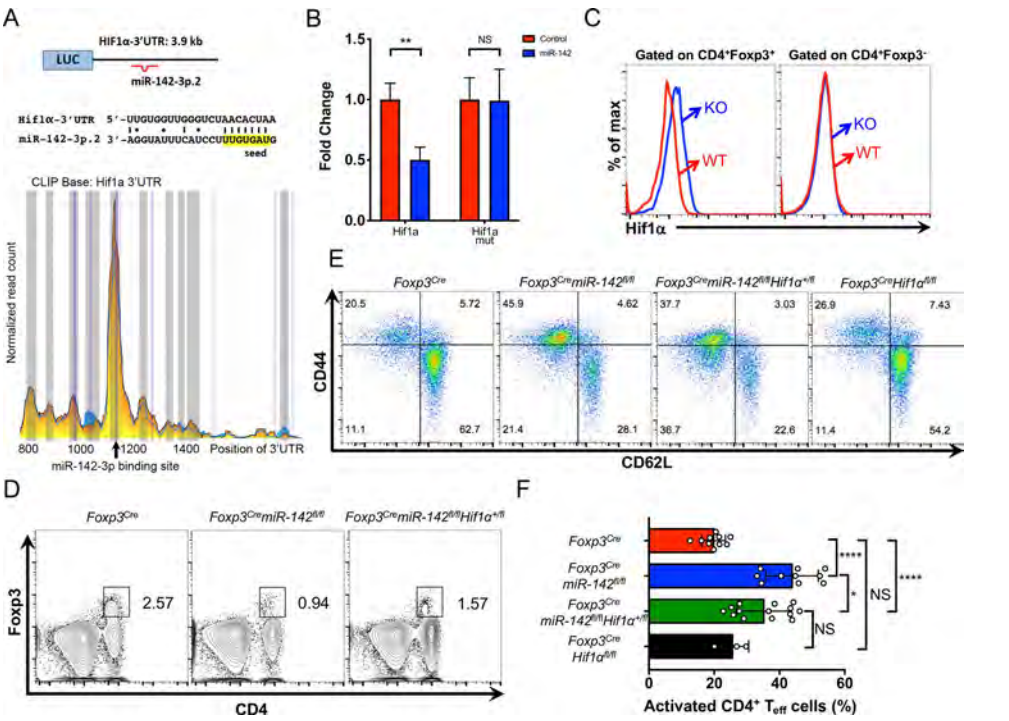

Fig 6. Lowering the *Hif1a* gene dose partially restores the normal size of T_{reg} population and attenuates hyperactivation of peripheral T cells in *Foxp3*^{Cre}*miR-142*$^{fl/fl}$ mice. (**A**) Diagram (top panel) and sequence alignment (middle panel) of miR-142-3p putative binding site in the *Hif1a* 3′ UTR. HITS-CLIP analysis (bottom panel) of Ago2 binding sites in the *Hif1a* 3′ UTR in activated CD4$^+$ T cells (blue plot, WT; yellow plot, *miR-155* KO). Note the peak of Ago2 binding activity that corresponds to the predicted miR-142-3p binding site (depicted by arrow). (**B**) Validation of *Hif1a* as direct miR-142-3p target by the 3′ UTR luciferase reporter assay. Relative expression of WT and miR-142-3p seed mutated *Hif1a* 3′ UTR reporter constructs upon cotransfection with either miR-142 precursor expressing plasmid or empty vector control. Expression of WT *Hif1a* 3′ UTR reporter in the presence of empty vector was arbitrarily set to 1. (**C**) Intracellular FACS analysis of Hif1α expression in CD4$^+$Foxp3$^+$ and CD4$^+$Foxp3$^-$ T cells from *Foxp3*^{Cre} (red line) and *Foxp3*^{Cre}*miR-142*$^{fl/fl}$ (blue line) spleens. (**D**) FACS analysis of splenic lymphocytes from 12- to 18-week-old *Foxp3*^{Cre}, *Foxp3*^{Cre}*miR-142*$^{fl/fl}$, and *Foxp3*^{Cre}*miR-142*$^{fl/fl}$*Hif1a*$^{+/fl}$ mice with anti-CD4 and anti-Foxp3 specific antibodies. Foxp3$^+$CD4$^+$ T_{reg} cells are gated, and numbers indicate the percentage of cells in the gate. (**E**) FACS analysis of CD44 and CD62L expression in splenic CD4$^+$ T cells from *Foxp3*^{Cre}, *Foxp3*^{Cre}*miR-142*$^{fl/fl}$, *Foxp3*^{Cre}*miR-142*$^{fl/fl}$*Hif1a*$^{+/fl}$, and *Foxp3*^{Cre}*Hif1a*$^{fl/fl}$ mice. Numbers indicate percentage of cells in the quadrants. (**F**) Frequency of activated (CD44$^+$CD62L$^-$) splenic CD4$^+$ T cells in *Foxp3*^{Cre} ($n = 10$), *Foxp3*^{Cre}*miR-142*$^{fl/fl}$ ($n = 10$), *Foxp3*^{Cre}miR-142$^{fl/fl}$*Hif1a*$^{+/fl}$ ($n = 14$), and *Foxp3*^{Cre}*Hif1a*$^{fl/fl}$ ($n = 3$) mice. Results are shown as mean ± SD. *P* values were calculated using 2-tailed Student *t* test. *, $P < 0.05$;**, $P < 0.01$; ****, $P < 0.0001$; NS, not significant. WT, *Foxp3*^{Cre}; KO, *Foxp3*^{Cre}*miR-142*$^{fl/fl}$. The underlying numerical raw data can be found in S1 Data file. The underlying flow cytometry raw data can be found at the Figshare repository. FACS, fluorescence activated cell sorting; *Hif1a*, hypoxia-induced factor 1 alpha; KO, knockout; SD, standard deviation; WT, wild-type.

https://doi.org/10.1371/journal.pbio.3001552.g006

in *Foxp3*^{Cre}*miR-142*$^{fl/fl}$ mice failed to ameliorate the lethal autoimmunity (S6C Fig), nor did *Hif1a* deletion restore the suppressive capacity (S6F and S6G Fig) of *miR-142*-deficient T_{reg} cells and attenuate the peripheral T_{eff} cell hyperactivation (S6H Fig), perhaps because of a failure to effectively rescue aberrant IFNγ production and signaling in T_{reg} cells (S6D and S6E Fig).

Discussion

Although miRNA-mediated posttranscriptional control of gene expression is recognized as crucial for T_{reg} cell development and function [11–13], our understanding of how specific miRNA genes govern T_{reg} cell responses is incomplete. Here, we report that mice with T_{reg} cell–specific *miR-142* deletion develop a fatal systemic autoimmune disease due to a severe defect in T_{reg} cell homeostasis and suppressive activity. Furthermore, we found that

constitutive *miR-142* ablation results in aberrant thymic T_{reg} cell development. Thus, our findings have uncovered an indispensable role for *miR-142* in the control of T_{reg} cell–mediated immunological tolerance. We propose that *miR-142* plays a dominant role among miRNAs involved in the regulation of T_{reg} cell activity because the phenotype of *Foxp3*^{Cre}*miR-142*$^{fl/fl}$ mice closely resembles the autoimmune pathology observed in mice with global disruption of miRNA biogenesis in T_{reg} cells [11–13]. This notion should be confirmed by further conditional KO studies of several miRNA genes that were previously implicated in the regulation of T_{reg} cell function, including *miR-146a*, *miR-155*, *and miR-27* [22,36,37].

The role of *miR-142* in T_{reg} cell function was previously examined by Anandagoda and colleagues using a conditional KO mouse model [20]. In contrast with the findings from this report, we determined that deletion of miR-142-3p and not miR-142-5p (as proposed by Anandagoda and colleagues) is the major driver of the T_{reg} cell defect and subsequent systemic autoimmunity in *Foxp3*^{Cre}*miR-142*$^{fl/fl}$ mice. This conclusion is strongly supported by the observed global derepression of miR-142-3p target genes in *miR-142*–deficient T_{reg} cells, whereas the levels of the majority of miR-142-5p targets did not significantly change. Our inference of a critical role for miR-142-3p in T_{reg} cells is well aligned with the fact that miR-142-3p is more abundantly expressed in T_{reg} cells than miR-142-5p and a large body of literature that assigns the main regulatory role in immune cells to miR-142-3p [14–18,28–30]. Our data revealing that miR-142-3p can directly bind and regulate the phosphodiesterase *Pde3b* gene, through which, as Anandagoda and colleagues suggest [20], *miR-142* controls T_{reg} cell immunosuppressive activity, further validates miR-142-3p as the key miR-142 isoform in T_{reg} cells.

Our findings indicate that miR-142-3p controls T_{reg} cell homeostasis and function by attenuating IFNγ production and signaling. Interestingly, dysregulation of IFNγ responses is increasingly recognized as a critical factor that negatively impacts T_{reg} cell activity. For example, excessive IFNγ production was reported to drive functional "fragility" of T_{reg} cells in the context of antitumor immunity [38]. Additionally, conditional deletion of the E3 ubiquitin ligase von Hippel–Lindau (*Vhl*) gene was shown to impair T_{reg} cell function through IFNγ dysregulation [35]. Moreover, unrestrained *Stat1* activation and subsequent IFNγ production by *Socs1*-deficient T_{reg} cells was linked to a severe failure of immunological tolerance [22]. Finally, a loss of functional activity by *Dicer*-deficient T_{reg} cells was associated with excessive IFNγ production [13].

miRNAs, despite eliciting a moderate effect on the expression of their target genes, often have a significant impact on cellular physiology through coordinated and coherent targeting of multiple key molecules in a signaling cascade [39]. In agreement with this notion, we found that *miR-142* is predicted to control expression of several IFNγ-associated genes, including *Ifngr2*, *Gbp3*, *Stat1*, *Irf1*, and *Hif1a* and validated some of these as *bona fide* miR-142-3p targets. We propose that coordinated derepression of these target genes in *miR-142*–deficient T_{reg} cells drives the observed dysregulation of IFNγ responses. In support of this hypothesis, we found that genetic blockade of IFNγ production rescues the homeostatic defect in *miR-142*–deficient T_{reg} cells and prevents development of systemic lymphoproliferative and autoimmune disorder in *Foxp3*^{Cre}*miR-142*$^{fl/fl}$ mice. Despite a complete restoration of normal T_{reg} cell frequency in *Foxp3*^{Cre}*miR-142*$^{fl/fl}$*Ifng*$^{-/-}$ mice, the partial rescue of peripheral T_{eff} cell hyperactivation in these mice suggests a possibility that *miR-142*–mediated control of T_{reg} cell function is not limited to the attenuation of IFNγ signaling and likely involves additional molecular targets. Another caveat of our genetic epistasis experiments using *Foxp3*^{Cre}*miR-142*$^{fl/fl}$*Ifng*$^{-/-}$ mice is a potential non–cell-autonomous effect of IFNγ deletion on *miR-142*–deficient T_{reg} cells. Because we found a significant IFNγ up-regulation in both *miR-142*–deficient T_{reg} cells and *miR-142*–sufficient T_{eff} cells in *Foxp3*^{Cre}*miR-142*$^{fl/fl}$ mice, the global IFNγ ablation might

potentially impact *miR-142*–deficient T_{reg} cell function in cell-extrinsic manner via changes in their IFNγ-rich inflammatory environment. Future analysis of *miR-142*–sufficient and *miR-142*–deficient T_{reg} cells from animals that lack IFNγ expression such as $Foxp3^{Cre}miR\text{-}142^{fl/fl}Ifng^{-/-}$ and female $Foxp3^{Cre/+}miR\text{-}142^{fl/fl}$ mice will be required to corroborate the intrinsic effect of IFNγ on *miR-142*-deficient T_{reg} cells and uncover the additional signaling pathways through which *miR-142* mediates its regulatory functions in T_{reg} cells.

Our investigation of *Hif1a*, a validated miR-142-3p target, revealed an important role for the *miR-142-Hif1a* axis in the regulation of T_{reg} cell homeostasis. We observed that lowering the *Hif1a* gene dose in *miR-142*–deficient T_{reg} cells partially rescued the T_{reg} homeostatic defect and modestly reduced the hyperactivation of peripheral T_{eff} cells in $Foxp3^{Cre}miR\text{-}142^{fl/fl}$ mice. The role suggested by our findings for *Hif1a* as a negative regulator of T_{reg} cell homeostasis is consistent with the conclusions of 2 previous reports [35,38]. However, *Hif1a* haploinsufficiency had little impact on the dysregulated IFNγ production in *miR-142*–deficient T_{reg} cells and failed to prevent development of fatal autoimmunity in $Foxp3^{Cre}miR\text{-}142^{fl/fl}$ mice. This outcome is not surprising given the fact that the T_{reg} cell number in $Foxp3^{Cre}miR\text{-}142^{fl/fl}Hif1a^{+/fl}$ mice is only partially restored. The failure of *Hif1a* haploinsufficiency to fully rescue the T_{reg} cell defect in $Foxp3^{Cre}miR\text{-}142^{fl/fl}$ mice is probably linked to the abundance of miR-142-3p target genes in the IFNγ signaling pathway. The existence of multiple miR-142-3p targets likely makes the dysregulated state of IFNγ signaling in *miR-142*–deficient T_{reg} cells refractory to changes in the expression of a single target. This conclusion is supported by studies in miR-142-3p-deficient zebra danio, which display impaired myelopoiesis due to an aberrant activation of the IFNγ signaling pathway [17]. This developmental defect in miR-142-3p-deficient zebra danio could be rescued by a compound knockdown of *stat1a* and *irf1b* genes, whereas silencing of either factor alone was insufficient to restore normal neutrophil differentiation. Of note, based on the observations of dysregulated IFNγ signaling in *miR-142*–deficient immune cells from zebra danio and rodents, the role of *miR-142* in suppressing IFNγ signaling appears to be evolutionary conserved. In contrast, the function of *miR-142-Pde3b* signaling axis is unlikely to be evolutionary preserved, because miR-142-3p and miR-142-5p binding sites in the mouse Pde3b 3′ UTR are poorly conserved.

In summary, our results have established *miR-142* as a central regulator of T_{reg} cell development, homeostasis, and suppressive activity that mediates its function in T_{reg} cells in part by limiting IFNγ production and responsiveness. Besides advancing our understanding of the T_{reg} cell biology, these novel insights may open a new avenue for targeted pharmacological manipulation of T_{reg} cell activity in cancer immunotherapy and autoimmune disease settings.

Materials and methods

Mice

C57BL/6J (stock#000664), B6/CD45.1 (stock#002014), $Hif1a^{fl/fl}$ (stock#007561), and $Foxp3^{YFP\text{-}Cre}$ (stock#016959) mice were purchased from the Jackson Laboratory (Bar Harbor, Maine, USA). BALB/c mice were obtained from Charles River Laboratories (Wilmington, Massachusetts, USA). $miR\text{-}142^{fl/fl}$ mice were described previously [14]. $Foxp3^{Cre}miR\text{-}142^{fl/fl}$ mice were generated by crossing $miR\text{-}142^{fl/fl}$ mice with $Foxp3^{YFP\text{-}Cre}$ deleter/reporter mice [21]. Mice were kept in a specific pathogen-free facility at the City of Hope Animal Resource Center, and all animal procedures were approved by the Institutional Animal Care and Use Committee (IACUC) of the City of Hope. Our approved animal protocols that are relevant for this work are the following: IACUC#13021, IACUC#13020, and IACUC#03008.

Flow cytometry

For surface marker analysis, single cell suspensions from thymus, spleen, and peripheral lymph nodes (axillary, brachial, inguinal, and cervical) were treated with red blood cell (RBC) lysis buffer (BioLegend, San Diego, California, USA) to eliminate mature erythrocytes and then blocked with anti-CD16/CD32 antibody (Ab) to prevent nonspecific binding. Cells were stained with monoclonal fluorophore-conjugated antibodies against specific cell surface markers, such as anti-CD4 (clone RM4-5), anti-CD8α (clone 53–6.7), anti-CD25 (clone PC61), anti-CD44 (clone IM7), anti-CD62L (clone MEL-14), anti-CD45.1 (clone A20), anti-ICOS (clone 7E.17G9), anti-GITR (clone DTA-1), anti-CTLA-4 (clone UC10-4B9), anti-PD-1 (clone 29F.1A12), and anti-CD103 (clone 2E7) antibodies (all from BioLegend). Intracellular staining with anti-Foxp3 (clone FJK-16s; eBioscience, Santa Clara, California, USA) and anti-Hif1α (clone 241812; R&D Systems, Minneapolis, Minnesota, USA) antibodies was performed using fixed and permeabilized cells following the manufacturer's protocol. For detection of phosphorylated Stat1 (pStat1), purified $CD4^+$ T cells were first stimulated with IFNγ (100 ng/mL) for 24 hours, fixed with Cytofix buffer and permeabilized with Phosflow Perm Buffer III, and subsequently stained with anti-pStat1 (Y701; clone 4a; BD Biosciences, San Jose, California, USA) antibodies. For intracellular cytokine staining, T cells derived from spleen and lymph nodes or purified T_{reg} cells were first stimulated with phorbol 12-myristate 13-acetate (PMA; 50 ng/mL) and ionomycin (500 ng/mL) for 4 hours in the presence of monensin (2 μM) and then fixed, permeabilized, and stained following the manufacturer's protocol (BioLegend). Data were acquired on Accuri C6 flow cytometer (BD Biosciences) and analyzed with FlowJo software BD Biosciences (San Jose, California, USA). Cell sorting for the analysis of *miR-142* expression in T-cell lineage was performed using FACSAriaIII (BD Biosciences) instrument.

All flow cytometry raw data generated in this study can be found at the Figshare data repository (https://figshare.com/projects/microRNA-142_guards_against_autoimmunity_by_controlling_Treg_cell_homeostasis_and_function/128960).

Global transcriptome profiling by RNA-seq

$CD4^+YFP^+$ T_{reg} cells were sorted using BD FACSAria II machine from single-cell splenocyte suspensions derived from 8- to 11-week-old $Foxp3^{Cre}$ and $Foxp3^{Cre}miR\text{-}142^{fl/fl}$ female mice ($n = 3$ per group). Total RNA from purified WT and *miR-142*–deficient T_{reg} cells was isolated using miRNeasy kit (QIAGEN, Hilden, Germany) and subjected to RNA-seq. RNA quality was determined with an Agilent Bioanalyzer (RNA integrity number (RIN) > 7.5 for all samples). Library was prepared according to the manufacturer's protocol using Illumina TruSeq RNA Library Prep Kit v2 (San Diego, Califonia, USA) and subsequently loaded on an Illumina HiSeq 2500 for parallel sequencing. The 51 base pair single-ended sequence reads were mapped to the mouse reference genome (mm10) using the alignment program HISAT (https://daehwankimlab.github.io/hisat2). Gene expression was measured from alignment bam files by read counting function featureCounts in the Bioconductor package Rsubread (http://bioconductor.org/packages/Rsubread). The unstranded raw counts were then normalized using a trimmed mean of M values (TMM) method implemented in the Bioconductor package edgeR (https://bioconductor.org/packages/edgeR). A total of 11,658 genes having counts per million (CPM) values higher than 1 in at least 3 samples were included in the downstream differential expression analysis. Differentially expressed genes were tested using 3 statistical methods in edgeR, including the generalized linear model (GLM) quasi-likelihood F (QLF) test, the likelihood ratio (LR) test, and the exact test based on quantile-adjusted conditional maximum likelihood (qCML) methods. A complete list of genes and the statistical test results (*miR-142*–deficient (KO) versus *miR-142*–sufficient (WT) T_{reg} cells) are shown in S1

Table. Statistical *P* values were adjusted by Benjamini–Hochberg method for false discovery rate (FDR) controls. The volcano plot visualizing the distribution of differentially expressed genes was based on QLF test results. The RNA-seq raw data were deposited in the Gene Expression Omnibus under the accession number GSE190192.

Pathway and GSEA

Differentially expressed genes passing the criterion of FDR lower than 0.05 for all 3 statistical methods mentioned above were subjected for pathway and GSEA using Enrichr (http://amp.pharm.mssm.edu/Enrichr) software algorithm [31]. Top ranked pathways across major databases, including Panther (http://www.pantherdb.org), Reactome (https://reactome.org), KEGG (https://www.genome.jp/kegg), and WikiPathways (https://www.wikipathways.org) were identified and are listed in S2 Table. In addition, GSEA analysis (http://software.broadinstitute.org/gsea/index.jsp)) [32] was performed with the CPM values from the 11,658 expressed genes rank-ordered by Signal2Noise metric. Gene ontology gene sets from Molecular Signatures Database (MSigDB) v7.1 were evaluated for the enrichment.

Sylamer analysis

Analysis of miRNA seed enrichment in the 3′ UTRs of genes that are differentially expressed in *miR-142* KO T_{reg} cells was performed by the Web-based SylArray software algorithm (http://www.ebi.ac.uk/enright-srv/sylarray)) [26].

In vitro T_{reg} cell suppression assay

$CD4^+$ T cells were isolated from $Foxp3^{Cre}$, $Foxp3^{Cre}miR\text{-}142^{fl/fl}$, and $Foxp3^{Cre}miR\text{-}142^{fl/fl}Hif1a^{fl/fl}$ spleens using anti-CD4-biotin (clone GK1.5), anti-Biotin MicroBeads (Miltenyi Bergisch, Gladbach, North Rhine-Westphalia, Germany), LS columns (Miltenyi), and a MiniMACS Separator (Miltenyi). Enriched $CD4^+$ T cells were sorted for YFP^+(T_{reg}) and YFP^-(T_{con}) cells using BD FACS Fusion. Moreover, 10^5 $Foxp3^{Cre}$ $CD4^+YFP^-$ T_{con} cells were labeled with 4μM CellTrace Violet (CTV) (Thermo Fisher, Waltham, Massachusetts, USA) at 37˚C for 7.5 minutes and cultured with either $Foxp3^{Cre}miR\text{-}142^{fl/fl}$ or $Foxp3^{Cre}miR\text{-}142^{fl/fl}Hif1a^{fl/fl}$ $CD4^+YFP^+$ T_{reg} cells at ratios of 1:0.5 and 1:0.125 in the presence of CD3ε/CD28-conjugated MACSiBead Particles (mouse T Cell Activation/Expansion Kit, Miltenyi) at a bead-to-cell ratio of 2:1. After 3 days of culturing, proliferation of $Foxp3^{Cre}$ $CD4^+YFP^-$ T_{con} cells was measured by flow cytometry as CTV dilution.

In vitro T_{reg} survival assay

$CD4^+$ T cells isolated from $Foxp3^{Cre}$ and $Foxp3^{Cre}miR\text{-}142^{fl/fl}$ spleens by EasySep Mouse $CD4^+$ T Cell Isolation Kit (STEMCELL Technologies, Vancouver, British Columbia, Canada) were sorted for YFP expressing cells using BD FACSAria II instrument. $CD4^+YFP^+$ T_{reg} cells were stimulated with anti-CD3 (1 μg/mL) specific antibodies for 48 hours, stained with Annexin V-PE (BioLegend) and analyzed by flow cytometry. For the IFNγ-induced apoptosis of T_{reg} cells assay, splenocytes were cultured for 24 hours in the presence or absence of IFNγ (10 ng/mL) and then harvested and stained with Annexin V-PE for fluorescence activated cell sorting (FACS) analysis.

In vivo labeling of T_{reg} cells with BrdU

$Foxp3^{Cre}$ and $Foxp3^{Cre}miR\text{-}142^{fl/fl}$ mice were injected intraperitoneally with 1 mg of BrdU and splenic $BrdU^+$ T_{reg} cells ($CD4^+YFP^+$) were quantified by flow cytometry 16 hours

postinjection. Intracellular staining with anti-BrdU specific antibodies was performed using BrdU Flow Kit (BD Biosciences).

aGVHD mouse model

BALB/c recipient mice were lethally irradiated (850 cGy) 8 to 10 hours prior to bone marrow transplantation (BMT) and subsequently transplanted via intravenous injection with T-cell–depleted bone marrow from C57BL/6J mice (TCD-BM, 2.5×10^6 cells), Thy1.2$^+$CD4$^+$ T cells from C57BL/6J spleens (0.5 to 0.6×10^6 cells), and CD4$^+$YFP$^+$ T_{reg} cells derived from either *Foxp3*^{Cre} or *Foxp3*^{Cre}*miR-142*$^{fl/fl}$ spleens (0.1 to 0.12×10^6 cells). Body weight and severity of diarrhea in host mice were monitored and recorded for 15 days after BMT. Donor T_{reg} cell frequency in the host spleen was assessed by FACS on day 17 after transplantation.

miRNA qRT-PCR

Total RNA was isolated using miRNeasy kit (QIAGEN) and reverse transcribed using the TaqMan MicroRNA Reverse Transcription Kit (Life Technologies, Carlsbad, California, USA). Mature miR-142-3p expression was assessed by TaqMan Real-Time miRNA assay (Life Technologies) and normalized to snoRNA234 levels.

3′ UTR luciferase reporter assays

DNA fragments encompassing WT and miR-142-3p seed mutated 3′ UTRs of mouse *Hif1a*, *Ifngr2*, and *Pde3b* genes were synthesized and cloned into pMIR-Report vector (Ambion, Austin, Texas, USA). The sequence complementary to the miR-142-3p.2 seed sequence (8-mer) in the *Ifngr2* 3′ UTR was mutated from 5′-AACACTAA-3′ to 5′-ACGTACCA-3′. The sequence complementary to the miR-142-3p.2 seed sequence (8-mer) in the *Hif1a* 3′ UTR was mutated from 5′- AACACTAA-3′ to 5′- ACGTACCA-3′. The sequence complementary to the miR-142-3p.1 seed sequence (6-mer) in the *Pde3b* 3′ UTR was mutated from 5′- CACTAC-3′ to 5′-CCAGCC-3′. To perform the 3′ UTR reporter assays, 10^5 293T cells in 24-well plates were transiently transfected using calcium phosphate with 10 ng of pMIR-Report-3′ UTR firefly luciferase plasmid, 20 ng of Renilla luciferase reporter plasmid (pRL-SV40; Promega, Madison, Wisconsin, USA), and 450 ng of either pMDH1-miR-142 or control pMDH1 vector (Addgene, Watertown, Massachusetts, USA). Cells were lysed 48 hours posttransfection, and the luciferase activities were assessed using Dual Luciferase Reporter assay (Promega).

IFNγ ELISA

CD4$^+$ T cells purified from *Foxp3*^{Cre} and *Foxp3*^{Cre}*miR-142*$^{fl/fl}$ splenocytes with the help of EasySep Mouse CD4$^+$ T Cell Isolation Kit (STEMCELL Technologies) were sorted for YFP expressing cells using BD FACSAria II instrument. CD4$^+$YFP$^+$ T_{reg} cells (10^6/mL) were stimulated with anti-CD3 (5 μg/mL) and anti-CD28 (2 μg/mL) specific antibodies for 48 hours in the presence of IL-2 (50 ng/mL) and cell culture supernatants were assessed for IFNγ production by sandwich ELISA. Briefly, 96-well flat-bottom Maxisorp (Thermo Fisher) plates were coated with anti-mouse IFNγ-specific capture antibodies (eBioscience, clone XMG1.2), and the captured mouse IFNγ was detected with biotin labeled anti-mouse IFNγ-specific antibodies (eBioscience, clone R4-6A2). Mouse recombinant IFNγ (eBioscience) was used as a standard to quantify the results.

Histopathology

For histological sectioning, mouse tissues were collected and placed into 10% formalin, fixed for 24 hours, washed, and transferred to 70% ethanol before standard paraffin embedding.

Tissue sections were stained with hematoxylin and eosin and examined by an experienced veterinary pathologist.

Statistical analysis

All statistical analyses were performed using Prism 6 (GraphPad, San Diego, California, USA) software. Statistical analyses were performed using 2-tailed Student *t* test or ANOVA. Results were considered significant when $P \leq 0.05$.

Supporting information

S1 Fig. *miR-142* expression in T-cell lineage and analysis of germline (*miR-142*$^{-/-}$) and T_{reg} cell–specific (*Foxp3*^{Cre}*miR-142*$^{fl/fl}$) *miR-142* KO mice. (**A**) Impaired T_{reg} cell development in *miR-142*$^{-/-}$ mice. Left panel, FACS analysis of WT and *miR-142*$^{-/-}$ thymocytes with anti-CD4 and anti-Foxp3 antibodies. Foxp3^{+}CD4^{+} T_{reg} cells are gated and numbers indicate the percentage of cells in the gate. Right panel, frequency of CD4^{+}Foxp3^{+} T_{reg} cells in WT and *miR-142*$^{-/-}$ thymi ($n = 3$ per group). (**B, C**) T_{reg} cell defect in the periphery of *miR-142*$^{-/-}$ mice. FACS analysis of T_{reg} cells in spleen (**B**) and MLNs (**C**) from WT and *miR-142*$^{-/-}$ mice. Right panel, frequency of CD4^{+}Foxp3^{+} T_{reg} cells in WT and *miR-142*$^{-/-}$ spleens and MLNs ($n = 4$ per group). (**D**) qRT-PCR analysis of mature miR-142-3p and miR-142-5p expression in different T-cell subsets purified from *Foxp3*^{Cre} mice ($n = 2$). DN, double negative CD4^{-}CD8^{-} thymocytes; DP, double positive CD4^{+}CD8^{+} thymocytes; SP, single positive CD4^{+}YFP^{-} thymocytes; T_{reg}, CD4^{+}YFP^{+} T_{reg} cells from thymus and spleen, respectively; T_{Naive}, naive CD4^{+}YFP^{-}CD62L^{+}CD44^{-} splenic T cells; $T_{Activated}$, activated CD4^{+}YFP^{-}CD62L^{-}CD44^{+} splenic T cells. Expression level of miR-142-3p in DN population was arbitrarily set to 1. snoRNA234 levels were used for normalization. (**E**) qRT-PCR analysis of mature miR-142-3p expression in CD4^{+}YFP^{+} T_{reg} and CD4^{+}YFP^{-} T_{eff} cells purified from *Foxp3*^{Cre} and *Foxp3*^{Cre}*miR-142*$^{fl/fl}$ spleens. Expression level of miR-142-3p in CD4^{+}YFP^{+} T_{reg} cells isolated from *Foxp3*^{Cre}*miR-142*$^{fl/fl}$ spleen was arbitrarily set to 1. snoRNA234 levels were used for normalization. Spleen (**F**) and thymus (**G**) weights in 8- to 11-week-old male *Foxp3*^{Cre} and *Foxp3*^{Cre}*miR-142*$^{fl/fl}$ mice ($n \geq 7$ per group). Absolute cell counts in spleen (**H**), thymus (**I**), and peripheral lymph nodes (**J**) from *Foxp3*^{Cre} and *Foxp3*^{Cre}*miR-142*$^{fl/fl}$ mice ($n = 6$ per group). Results are shown as mean ± SD. *P* values were calculated using 2-tailed Student *t* test. **, $P < 0.01$; ***, $P < 0.001$; ****, $P < 0.0001$; NS, not significant. The underlying numerical raw data can be found in S1 Data file. The underlying flow cytometry raw data can be found at the Figshare repository. FACS, fluorescence activated cell sorting; KO, knockout; MLN, mesenteric lymph node; PLN, peripheral lymph node; SD, standard deviation; SP, spleen; T_{reg}, regulatory T; WT, wild-type; YFP, yellow fluorescent protein.
(PDF)

S2 Fig. Characterization of T_{reg} and T_{eff} cell defects in *Foxp3*^{Cre}*miR-142*$^{fl/fl}$mice. (**A**) FACS analysis of lymphocytes from PLNs (left panel) and thymus (right panel) of 12-week-old *Foxp3*^{Cre}and *Foxp3*^{Cre}*miR-142*$^{fl/fl}$ mice with anti-CD4 and anti-Foxp3 specific antibodies. Foxp3^{+}CD4^{+} T_{reg} cells are gated and numbers indicate the percentage of cells in the gate. (**B**) Frequency (left panel) and total number (right panel) of T_{reg} cells in PLNs and thymi of 12-week-old *Foxp3*^{Cre} (red bars) and *Foxp3*^{Cre}*miR-142*$^{fl/fl}$ (blue bars) mice ($n = 3$ per group). (**C**) FACS analysis of CD44 and CD62L expression on CD4^{+} (upper panel) and CD8^{+} (bottom panel) T cells from *Foxp3*^{Cre} and *Foxp3*^{Cre}*miR-142*$^{fl/fl}$ PLNs. Numbers indicate percentage of cells in the quadrants. (**D**) Frequency of CD44^{-}CD62L^{+} (naive) and CD44^{+}CD62L^{-} (activated) CD4^{+} (left panel) and CD8^{+} (right panel) T cells in *Foxp3*^{Cre} and *Foxp3*^{Cre}*miR-142*$^{fl/fl}$ PLNs

($n = 6$ per group). (**E**) Intracellular FACS analysis of IFNγ production by $CD4^+$ (upper panel) and $CD8^+$ (bottom panel) T cells from $Foxp3^{Cre}$ and $Foxp3^{Cre}miR\text{-}142^{fl/fl}$ PLNs. $IFN\gamma^+$ T cells are gated and numbers indicate percentage of cells in the gate. (**F**) Frequency of IFNγ-expressing $CD4^+$ and $CD8^+$ T cells in $Foxp3^{Cre}$ (filled bars) and $Foxp3^{Cre}miR\text{-}142^{fl/fl}$ (open bars) PLNs ($n = 4$ per group). (**G**) Total $CD4^+$ and $CD8^+$ T cell counts in $Foxp3^{Cre}$ (filled bars) and $Foxp3^{Cre}miR\text{-}142^{fl/fl}$ (open bars) PLNs ($n = 6$ per group). (**H**) Frequencies of IFNγ-, IL-4-, and IL-17-expressing $CD4^+$ T cells isolated from $Foxp3^{Cre}$ (filled bars) and $Foxp3^{Cre}miR\text{-}142^{fl/fl}$ (open bars) spleens ($n \geq 3$ per group). Results are shown as mean ± SD. *P* values were calculated using 2-tailed Student *t* test. *, $P < 0.05$; **, $P < 0.01$; ***, $P < 0.001$; ****, $P < 0.0001$; NS, not significant. The underlying numerical raw data can be found in S1 Data file. The underlying flow cytometry raw data can be found at the Figshare repository. FACS, fluorescence activated cell sorting; IFNγ, interferon gamma; IL, interleukin; PLN, peripheral lymph node; SD, standard deviation; T_{reg}, regulatory T.
(PDF)

S3 Fig. Immunophenotyping of *miR-142*–deficient T_{reg} cells. (**A**) FACS analysis of T_{reg} suppression activity in vitro. Purified $CD4^+$ T_{conv} cells were loaded with CTV dye and incubated with FACS-sorted T_{reg} cells from $Foxp3^{Cre}$ (red line) and $Foxp3^{Cre}miR\text{-}142^{fl/fl}$ (blue line) spleens in the presence of beads coated with anti-CD3 and anti-CD28 specific antibodies. Several T_{reg} to T_{conv} cell ratios were shown as indicated. (**B**) Left panel, FACS analysis of Annexin V-stained $CD4^+YFP^+$ T_{reg} cells from $Foxp3^{Cre}$ (WT) or $Foxp3^{Cre}miR\text{-}142^{fl/fl}$ (KO) spleens. Right panel, MFI of Annexin V staining on T_{reg} cells from $Foxp3^{Cre}$ (WT) or $Foxp3^{Cre}miR\text{-}142^{fl/fl}$ (KO) spleens. (**C**) Frequency of splenic YFP^+ T_{reg} cells in female $Foxp3^{Cre/WT}miR\text{-}142^{+/+}$ and $Foxp3^{Cre/WT}miR\text{-}142^{fl/fl}$ mice. (**D**) MFI of GITR, CD25, CD103, PD-1, CTLA-4, and ICOS expression on splenic $CD4^+YFP^+$ T_{reg} cells from $Foxp3^{Cre}$ (WT) or $Foxp3^{Cre}miR\text{-}142^{fl/fl}$ (KO) mice. Results are shown as mean ± SD. *P* values were calculated using 2-tailed Student *t* test *, $P < 0.05$; **, $P < 0.01$; NS, not significant. The underlying numerical raw data can be found in S1 Data file. The underlying flow cytometry raw data can be found at the Figshare repository. CTV, cell trace violet; FACS, fluorescence activated cell sorting; KO, knockout; MFI, mean fluorescence intensity; T_{reg}, regulatory T; WT, wild-type; YFP, yellow fluorescent protein.
(PDF)

S4 Fig. Gene expression signatures in *miR-142*–deficient T_{reg} cells. Heatmap visualization of differentially expressed cytokine, chemokine, and immune receptor genes (**A**) and T_{reg} cell signature genes (**B**). Genes highlighted in red are putative miR-142-3p targets. (**C**) Standard enrichment plot demonstrating the enrichment of up-regulated genes in *miR-142*–deficient T_{reg} cells from gene ontology term "regulation of response to interferon gamma" using the GSEA tool. (**D**) ELISA analysis of IFNγ production by $Foxp3^{Cre}$ (WT) and $Foxp3^{Cre}miR\text{-}142^{fl/fl}$ (KO) T_{reg} cells ($n = 4$ per group). Purified $CD4^+YFP^+$ T_{reg} cells (10^6/mL) were stimulated with anti-CD3 (5 μg/ml) and anti-CD28 (2 μg/ml) antibodies in the presence of IL-2 (50 ng/ml) for 48 hours. (**E**) MFI of phospho-Stat1(Y701) levels in $Foxp3^{Cre}$ (WT; $n = 6$) and $Foxp3^{Cre}miR\text{-}142^{fl/fl}$ (KO; $n = 5$) T_{reg} cells. *P* values were calculated using 2-tailed Student *t* test. *, $P < 0.05$; **, $P < 0.01$. The underlying raw data can be found in S1 Data file. GSEA, Gene Set Enrichment Analysis; IFNγ, interferon gamma; IL, interleukin; KO, knockout; MFI, mean fluorescence intensity; T_{reg}, regulatory T; WT, wild-type; YFP, yellow fluorescent protein.
(PDF)

S5 Fig. Characterization of the molecular mechanism by which *miR-142* controls T_{reg} cell homeostasis and function. (**A**) Diagrams (top left) and sequence alignments (top right) of

putative miR-142-3p binding sites in the 3′ UTRs of *Stat1*, *Ifngr2*, *Irf1*, *Gbp3*, and *Pde3b* genes. HITS-CLIP analysis of Ago2 binding to the 3′ UTRs of *Ifngr2* (bottom-left) and *Gbp3* (bottom-right) genes in WT (blue plot) and *miR-155* KO (yellow plot) activated $CD4^+$ T cells. Sequences corresponding to miR-142-3p binding sites are labeled by arrows. (**B**) Validation of *Pde3b* and *Ifngr2* as direct miR-142-3p targets by the 3′ UTR luciferase reporter assay ($n = 2$). Relative expression of WT and miR-142-3p seed mutated *Pde3b* and *Ifngr2* 3′ UTR reporter constructs upon cotransfection with either miR-142 precursor expressing plasmid or empty vector control. Expression of WT *Pde3b* and *Ifngr2* 3′ UTR reporters in the presence of empty vector were set to 1. (**C**) MFI of Hif1α in $Foxp3^{Cre}$ (WT; red bars) and $Foxp3^{Cre}miR\text{-}142^{fl/fl}$ (KO; blue bars) $CD4^+Foxp3^+$ T_{reg} and $CD4^+Foxp3^-$ T_{conv} cells ($n = 6$ per group). (**D**) Left panel, FACS analysis of IFNγR2 expression in $CD4^+YFP^+$ T cells from $Foxp3^{Cre}$ (red line) and $Foxp3^{Cre}miR\text{-}142^{fl/fl}$ (blue line) spleens; right panel, MFI of IFNγR2 in $Foxp3^{Cre}$ (WT; red bars) and $Foxp3^{Cre}miR\text{-}142^{fl/fl}$ (KO; blue bars) $CD4^+YFP^+$ T_{reg} cells. (**E**) Schematic diagram and sequence conservation of 2 miR-142-5p and one miR-142-3p binding sites in the 3′ UTR of mouse *Pde3b* gene as determined by the TargetScan algorithm. (**F**) Sequence alignment of miR-142-3p binding sites in mouse Pde3b-WT and Pde3b-MUT 3′ UTR reporter constructs. Results are shown as mean ± SD. *P* values were calculated using 2-tailed Student *t* test. *, $P < 0.05$; **, $P < 0.01$; ***, $P < 0.001$; NS, not significant. The underlying numerical raw data can be found in S1 Data file. The underlying flow cytometry raw data can be found at the Figshare repository. FACS, fluorescence activated cell sorting; IFNγ, interferon gamma; KO, knockout; MFI, mean fluorescence intensity; SD, standard deviation; T_{reg}, regulatory T; WT, wild-type; YFP, yellow fluorescent protein.
(PDF)

S6 Fig. Phenotypic analysis of $Foxp3^{Cre}miR\text{-}142^{fl/fl}Hif1a^{+/fl}$ and $Foxp3^{Cre}miR\text{-}142^{fl/fl}Hif1a^{fl/fl}$ mice. (**A**) Relative Hif1α protein expression in $Foxp3^{Cre}$ (WT; red bar), $Foxp3^{Cre}miR\text{-}142^{fl/fl}$ (KO; blue bar), and $Foxp3^{Cre}miR\text{-}142^{fl/fl}Hif1a^{+/fl}$ (HET; green bar) T_{reg} cells. The Hif1α levels in WT T_{reg} cells were arbitrarily set to 1. (**B**) Frequency of $CD4^+Foxp3^+$ T_{reg} cells in splenic lymphocytes from $Foxp3^{Cre}$ (WT; red bar; $n = 7$), $Foxp3^{Cre}miR\text{-}142^{fl/fl}$ (KO; blue bar; $n = 5$) and $Foxp3^{Cre}miR\text{-}142^{fl/fl}Hif1a^{+/fl}$ (HET; green bar; $n = 3$) mice. (**C**) Kaplan–Meier survival curves for $Foxp3^{Cre}$ (red line; $n = 27$), $Foxp3^{Cre}miR\text{-}142^{fl/fl}$ (blue line; $n = 27$), and $Foxp3^{Cre}miR\text{-}142^{fl/fl}Hif1a^{+/fl}$ (green line; $n = 8$) mice. Analysis of IFNγ production (**D**) and Stat1 activation (**E**) in T_{reg} cells from $Foxp3^{Cre}miR\text{-}142^{fl/fl}Hif1a^{+/fl}$ mice. Left panels, intracellular FACS analysis of splenic $CD4^+Foxp3^+$ T_{reg} cells from $Foxp3^{Cre}$ (red line; WT), $Foxp3^{Cre}miR\text{-}142^{fl/fl}$ (blue line; KO) and $Foxp3^{Cre}miR\text{-}142^{fl/fl}Hif1a^{+/fl}$ (green line; HET) mice with anti-IFNγ (**D**) and anti-pStat1 (Y701) (**E**) antibodies. Right panels, MFI of IFNγ and phospho-Stat1 (pSTAT1) in $Foxp3^{Cre}$ (WT; red bar), $Foxp3^{Cre}miR\text{-}142^{fl/fl}$ (KO; blue bar) and $Foxp3^{Cre}miR\text{-}142^{fl/fl}Hif1a^{+/fl}$ (HET; green bar) T_{reg} cells. (**F, G**) FACS analysis of immunosuppressive activity of T_{reg} cells derived from $Foxp3^{Cre}$ (WT; red dot), $Foxp3^{Cre}miR\text{-}142^{fl/fl}$ (KO; blue dot) and $Foxp3^{Cre}miR\text{-}142^{fl/fl}Hif1a^{fl/fl}$ (DKO; green dot) mice ($n = 3$) in vitro. Several T_{reg} to T_{conv} cell ratios were analyzed as indicated in the graph. Unstimulated T_{conv} cells were used as control. Representative FACS plot analysis is shown in G. (**H**) FACS analysis of CD44 and CD62L expression in splenic $CD4^+$ T cells from $Foxp3^{Cre}$, $Foxp3^{Cre}miR\text{-}142^{fl/fl}Hif1a^{+/fl}$, and $Foxp3^{Cre}miR\text{-}142^{fl/fl}Hif1a^{fl/fl}$ mice. Numbers indicate percentage of cells in the quadrants. Results are shown as mean ± SD. *P* values were calculated using 2-tailed Student *t* test. *, $P < 0.05$; **, $P < 0.01$; ****, $P < 0.0001$; NS, not significant. The underlying numerical raw data can be found in S1 Data file. The underlying flow cytometry raw data can be found at the Figshare repository. DKO, double knockout; FACS, fluorescence activated cell sorting; IFNγ, interferon gamma; KO, knockout; MFI, mean fluorescence intensity; pStat1, phosphorylated

Stat1; SD, standard deviation; T_{reg}, regulatory T; WT, wild-type.
(PDF)

S1 Data. Data underlying figures.
(XLSX)

S1 Table. Differentially expressed genes in *miR-142*–deficient T_{reg} cells. T_{reg}, regulatory T.
(XLSX)

S2 Table. Pathway enrichment analysis by Enrichr.
(XLSX)

Acknowledgments

We would like to thank Dr. Zuoming Sun and members of the Boldin laboratory at the City of Hope for helpful discussions and suggestions regarding the manuscript. We thank the City of Hope Animal Research Center for their help and care in breeding and maintaining our mouse colonies.

Author Contributions

Conceptualization: Wei-Le Wang, Mark P. Boldin.

Data curation: Wei-Le Wang, Ching Ouyang.

Formal analysis: Wei-Le Wang, Ching Ouyang, Natalie M. Graham, Yuankun Zhang, Mark P. Boldin.

Funding acquisition: Wei-Le Wang, Defu Zeng, Mark P. Boldin.

Investigation: Wei-Le Wang, Natalie M. Graham, Yuankun Zhang, Kaniel Cassady, Estefany Y. Reyes, Min Xiong, Alicia M. Davis, Kathie Tang, Mark P. Boldin.

Methodology: Wei-Le Wang, Natalie M. Graham, Yuankun Zhang, Kaniel Cassady, Estefany Y. Reyes, Min Xiong, Alicia M. Davis, Kathie Tang, Mark P. Boldin.

Project administration: Defu Zeng, Mark P. Boldin.

Resources: Wei-Le Wang, Ching Ouyang, Defu Zeng, Mark P. Boldin.

Software: Wei-Le Wang, Ching Ouyang, Mark P. Boldin.

Supervision: Defu Zeng, Mark P. Boldin.

Validation: Wei-Le Wang, Ching Ouyang, Natalie M. Graham, Yuankun Zhang, Kaniel Cassady, Estefany Y. Reyes, Min Xiong, Alicia M. Davis, Kathie Tang, Mark P. Boldin.

Visualization: Wei-Le Wang, Ching Ouyang, Mark P. Boldin.

Writing – original draft: Wei-Le Wang, Mark P. Boldin.

Writing – review & editing: Wei-Le Wang, Ching Ouyang, Natalie M. Graham, Mark P. Boldin.

References

1. Josefowicz SZ, Lu LF, Rudensky AY. Regulatory T cells: mechanisms of differentiation and function. Annu Rev Immunol. 2012; 30:531–64. https://doi.org/10.1146/annurev.immunol.25.022106.141623 PMID: 22224781.

2. Sakaguchi S, Yamaguchi T, Nomura T, Ono M. Regulatory T cells and immune tolerance. Cell. 2008; 133(5):775–87. https://doi.org/10.1016/j.cell.2008.05.009 PMID: 18510923.
3. Bennett CL, Christie J, Ramsdell F, Brunkow ME, Ferguson PJ, Whitesell L, et al. The immune dysregulation, polyendocrinopathy, enteropathy, X-linked syndrome (IPEX) is caused by mutations of FOXP3. Nat Genet. 2001; 27(1):20–1. https://doi.org/10.1038/83713 PMID: 11137993.
4. Fontenot JD, Gavin MA, Rudensky AY. Foxp3 programs the development and function of CD4+CD25+ regulatory T cells. Nat Immunol. 2003; 4(4):330–6. https://doi.org/10.1038/ni904 PMID: 12612578.
5. Hori S, Nomura T, Sakaguchi S. Control of regulatory T cell development by the transcription factor Foxp3. Science. 2003; 299(5609):1057–61. https://doi.org/10.1126/science.1079490 PMID: 12522256.
6. Khattri R, Cox T, Yasayko SA, Ramsdell F. An essential role for Scurfin in CD4+CD25+ T regulatory cells. Nat Immunol. 2003; 4(4):337–42. https://doi.org/10.1038/ni909 PMID: 12612581.
7. Wildin RS, Ramsdell F, Peake J, Faravelli F, Casanova JL, Buist N, et al. X-linked neonatal diabetes mellitus, enteropathy and endocrinopathy syndrome is the human equivalent of mouse scurfy. Nat Genet. 2001; 27(1):18–20. https://doi.org/10.1038/83707 PMID: 11137992.
8. Chen W, Jin W, Hardegen N, Lei KJ, Li L, Marinos N, et al. Conversion of peripheral CD4+CD25- naive T cells to CD4+CD25+ regulatory T cells by TGF-beta induction of transcription factor Foxp3. J Exp Med. 2003; 198(12):1875–86. https://doi.org/10.1084/jem.20030152 PMID: 14676299; PubMed Central PMCID: PMC2194145
9. Davidson TS, DiPaolo RJ, Andersson J, Shevach EM. Cutting Edge: IL-2 is essential for TGF-beta-mediated induction of Foxp3+ T regulatory cells. J Immunol. 2007; 178(7):4022–6. https://doi.org/10.4049/jimmunol.178.7.4022 PMID: 17371955.
10. Haribhai D, Williams JB, Jia S, Nickerson D, Schmitt EG, Edwards B, et al. A requisite role for induced regulatory T cells in tolerance based on expanding antigen receptor diversity. Immunity. 2011; 35(1):109–22. https://doi.org/10.1016/j.immuni.2011.03.029 PMID: 21723159; PubMed Central PMCID: PMC3295638
11. Chong MM, Rasmussen JP, Rudensky AY, Littman DR. The RNAseIII enzyme Drosha is critical in T cells for preventing lethal inflammatory disease. J Exp Med. 2008; 205(9):2005–17. https://doi.org/10.1084/jem.20081219 PMID: 18725527; PubMed Central PMCID: PMC2526196
12. Liston A, Lu LF, O'Carroll D, Tarakhovsky A, Rudensky AY. Dicer-dependent microRNA pathway safeguards regulatory T cell function. J Exp Med. 2008; 205(9):1993–2004. https://doi.org/10.1084/jem.20081062 PMID: 18725526; PubMed Central PMCID: PMC2526195
13. Zhou X, Jeker LT, Fife BT, Zhu S, Anderson MS, McManus MT, et al. Selective miRNA disruption in T reg cells leads to uncontrolled autoimmunity. J Exp Med. 2008; 205(9):1983–91. https://doi.org/10.1084/jem.20080707 PMID: 18725525; PubMed Central PMCID: PMC2526194
14. Kramer NJ, Wang WL, Reyes EY, Kumar B, Chen CC, Ramakrishna C, et al. Altered lymphopoiesis and immunodeficiency in miR-142 null mice. Blood. 2015; 125(24):3720–30. Epub 2015/05/02. https://doi.org/10.1182/blood-2014-10-603951 PMID: 25931583.
15. Chapnik E, Rivkin N, Mildner A, Beck G, Pasvolsky R, Metzl-Raz E, et al. miR-142 orchestrates a network of actin cytoskeleton regulators during megakaryopoiesis. Elife. 2014; 3:e01964. Epub 2014/05/27. https://doi.org/10.7554/eLife.01964 PMID: 24859754; PubMed Central PMCID: PMC4067751.
16. Mildner A, Chapnik E, Manor O, Yona S, Kim KW, Aychek T, et al. Mononuclear phagocyte miRNome analysis identifies miR-142 as critical regulator of murine dendritic cell homeostasis. Blood. 2013; 121(6):1016–27. https://doi.org/10.1182/blood-2012-07-445999 PMID: 23212522.
17. Fan HB, Liu YJ, Wang L, Du TT, Dong M, Gao L, et al. miR-142-3p acts as an essential modulator of neutrophil development in zebrafish. Blood. 2014; 124(8):1320–30. https://doi.org/10.1182/blood-2013-12-545012 PMID: 24990885.
18. Mildner A, Chapnik E, Varol D, Aychek T, Lampl N, Rivkin N, et al. MicroRNA-142 controls thymocyte proliferation. Eur J Immunol. 2017; 47(7):1142–52. https://doi.org/10.1002/eji.201746987 PMID: 28471480.
19. Sun Y, Oravecz-Wilson K, Mathewson N, Wang Y, McEachin R, Liu C, et al. Mature T cell responses are controlled by microRNA-142. J Clin Invest. 2015; 125(7):2825–40. https://doi.org/10.1172/JCI78753 PMID: 26098216; PubMed Central PMCID: PMC4563679
20. Anandagoda N, Willis JC, Hertweck A, Roberts LB, Jackson I, Gokmen MR, et al. microRNA-142-mediated repression of phosphodiesterase 3B critically regulates peripheral immune tolerance. J Clin Invest. 2019; 129(3):1257–71. Epub 2019/02/12. https://doi.org/10.1172/JCI124725 PMID: 30741720; PubMed Central PMCID: PMC6391082.
21. Rubtsov YP, Rasmussen JP, Chi EY, Fontenot J, Castelli L, Ye X, et al. Regulatory T cell-derived interleukin-10 limits inflammation at environmental interfaces. Immunity. 2008; 28(4):546–58. https://doi.org/10.1016/j.immuni.2008.02.017 PMID: 18387831.

22. Lu LF, Boldin MP, Chaudhry A, Lin LL, Taganov KD, Hanada T, et al. Function of miR-146a in controlling Treg cell-mediated regulation of Th1 responses. Cell. 2010; 142(6):914–29. Epub 2010/09/21. https://doi.org/10.1016/j.cell.2010.08.012 PMID: 20850013; PubMed Central PMCID: PMC3049116.

23. Lyszkiewicz M, Winter SJ, Witzlau K, Fohse L, Brownlie R, Puchalka J, et al. miR-181a/b-1 controls thymic selection of Treg cells and tunes their suppressive capacity. PLoS Biol. 2019; 17(3):e2006716. Epub 2019/03/12. https://doi.org/10.1371/journal.pbio.2006716 PMID: 30856173; PubMed Central PMCID: PMC6428341.

24. Cretney E, Kallies A, Nutt SL. Differentiation and function of Foxp3(+) effector regulatory T cells. Trends Immunol. 2013; 34(2):74–80. https://doi.org/10.1016/j.it.2012.11.002 PMID: 23219401.

25. Asano T, Meguri Y, Yoshioka T, Kishi Y, Iwamoto M, Nakamura M, et al. PD-1 modulates regulatory T-cell homeostasis during low-dose interleukin-2 therapy. Blood. 2017; 129(15):2186–97. https://doi.org/10.1182/blood-2016-09-741629 PMID: 28151427; PubMed Central PMCID: PMC5391624

26. Bartonicek N, Enright AJ. SylArray: a web server for automated detection of miRNA effects from expression data. Bioinformatics. 2010; 26(22):2900–1. https://doi.org/10.1093/bioinformatics/btq545 PMID: 20871108.

27. Chen J, Bardes EE, Aronow BJ, Jegga AG. ToppGene Suite for gene list enrichment analysis and candidate gene prioritization. Nucleic Acids Res. 2009; 37(Web Server issue):W305–11. https://doi.org/10.1093/nar/gkp427 PMID: 19465376; PubMed Central PMCID: PMC2703978.

28. Gao J, Gu J, Pan X, Gan X, Ju Z, Zhang S, et al. Blockade of miR-142-3p promotes anti-apoptotic and suppressive function by inducing KDM6A-mediated H3K27me3 demethylation in induced regulatory T cells. Cell Death Dis. 2019; 10(5):332. Epub 2019/04/17. https://doi.org/10.1038/s41419-019-1565-6 PMID: 30988391; PubMed Central PMCID: PMC6465300.

29. Huang B, Zhao J, Lei Z, Shen S, Li D, Shen GX, et al. miR-142-3p restricts cAMP production in CD4+CD25- T cells and CD4+CD25+ TREG cells by targeting AC9 mRNA. EMBO Rep. 2009; 10(2):180–5. Epub 2008/12/23. https://doi.org/10.1038/embor.2008.224 PMID: 19098714; PubMed Central PMCID: PMC2637310.

30. Lu Y, Gao J, Zhang S, Gu J, Lu H, Xia Y, et al. miR-142-3p regulates autophagy by targeting ATG16L1 in thymic-derived regulatory T cell (tTreg). Cell Death Dis. 2018; 9(3):290. Epub 2018/02/21. https://doi.org/10.1038/s41419-018-0298-2 PMID: 29459719; PubMed Central PMCID: PMC5833855.

31. Chen EY, Tan CM, Kou Y, Duan Q, Wang Z, Meirelles GV, et al. Enrichr: interactive and collaborative HTML5 gene list enrichment analysis tool. BMC Bioinformatics. 2013; 14:128. Epub 2013/04/17. https://doi.org/10.1186/1471-2105-14-128 PMID: 23586463; PubMed Central PMCID: PMC3637064.

32. Subramanian A, Tamayo P, Mootha VK, Mukherjee S, Ebert BL, Gillette MA, et al. Gene set enrichment analysis: a knowledge-based approach for interpreting genome-wide expression profiles. Proc Natl Acad Sci U S A. 2005; 102(43):15545–50. https://doi.org/10.1073/pnas.0506580102 PMID: 16199517; PubMed Central PMCID: PMC1239896

33. Agarwal V, Bell GW, Nam JW, Bartel DP. Predicting effective microRNA target sites in mammalian mRNAs. Elife. 2015;4. Epub 2015/08/13. https://doi.org/10.7554/eLife.05005 PMID: 26267216; PubMed Central PMCID: PMC4532895.

34. Loeb GB, Khan AA, Canner D, Hiatt JB, Shendure J, Darnell RB, et al. Transcriptome-wide miR-155 binding map reveals widespread noncanonical microRNA targeting. Mol Cell. 2012; 48(5):760–70. https://doi.org/10.1016/j.molcel.2012.10.002 PMID: 23142080; PubMed Central PMCID: PMC3562697

35. Lee JH, Elly C, Park Y, Liu YC. E3 Ubiquitin Ligase VHL Regulates Hypoxia-Inducible Factor-1alpha to Maintain Regulatory T Cell Stability and Suppressive Capacity. Immunity. 2015; 42(6):1062–74. https://doi.org/10.1016/j.immuni.2015.05.016 PMID: 26084024; PubMed Central PMCID: PMC4498255

36. Cruz LO, Hashemifar SS, Wu CJ, Cho S, Nguyen DT, Lin LL, et al. Excessive expression of miR-27 impairs Treg-mediated immunological tolerance. J Clin Invest. 2017; 127(2):530–42. https://doi.org/10.1172/JCI88415 PMID: 28067667; PubMed Central PMCID: PMC5272185

37. Lu LF, Thai TH, Calado DP, Chaudhry A, Kubo M, Tanaka K, et al. Foxp3-dependent microRNA155 confers competitive fitness to regulatory T cells by targeting SOCS1 protein. Immunity. 2009; 30(1):80–91. https://doi.org/10.1016/j.immuni.2008.11.010 PMID: 19144316; PubMed Central PMCID: PMC2654249

38. Overacre-Delgoffe AE, Chikina M, Dadey RE, Yano H, Brunazzi EA, Shayan G, et al. Interferon-gamma Drives Treg Fragility to Promote Anti-tumor Immunity. Cell 2017; 169(6):1130–41 e11. https://doi.org/10.1016/j.cell.2017.05.005 PMID: 28552348; PubMed Central PMCID: PMC5509332.

39. Inui M, Martello G, Piccolo S. MicroRNA control of signal transduction. Nat Rev Mol Cell Biol. 2010; 11(4):252–63. https://doi.org/10.1038/nrm2868 PMID: 20216554.